# REGULATORY, INTEGRATIVE AND COMPARATIVE PHYSIOLOGY.

Am J Physiol Regul Integr Comp Physiol 329: R555–R575, 2025. First published May 19, 2025; doi:10.1152/ajpregu.00236.2024

# **RESEARCH ARTICLE**

# The molecular origin of body temperature in homeothermic species

© Gerhard M. Artmann,¹ Oliver H. Weiergräber,² © Samar Damiati,³ © Ipek Seda Firat,¹ and Aysegül T. Artmann¹

<sup>1</sup>Center of Competence for Bioengineering, University of Applied Sciences Aachen, Medical and Biological Laboratory, Jülich, Germany; <sup>2</sup>Institute of Biological Information Processing, Structural Biochemistry (IBI-7), Forschungszentrum Jülich, Jülich, Germany; and <sup>3</sup>Department of Chemistry, College of Sciences, University of Sharjah, Sharjah, United Arab Emirates

#### **Abstract**

We propose the interfacial water quantum-transition (IWQ) model as a novel paradigm explaining temperature-dependent structural and functional transitions (discontinuities) observed in proteins. The central postulate states that experimentally measured critical temperatures,  $T_C$ , are related to physical reference temperatures,  $T_W$ , defined by rotational quantum transitions of temporarily free water molecules in the protein-water interface. Applicability of this concept is demonstrated with transitions observed in two disparate model systems, viz., hemoglobin and thermosensitive transient receptor potential (TRP) channels. We propose that the same mechanism underlies the definition of basal body temperatures in homeotherms, the reference temperature for humans being  $T_W = 36.32^{\circ}C$ . Specifically, we demonstrate that the body temperatures of both human and chicken (representing the two classes of homeothermic vertebrates) not only coincide with quantum-transition reference temperatures but are also related to pronounced transitions in hemoglobin oxygen saturation. This suggests that the evolution of body temperatures in different homeothermic species might involve an interplay between critical parameters of oxygen supply on the one hand and quantum-physical rotational transition temperatures of water on the other. Casting the IWQ model concept into a concise formula: Proteins sense and water sets critical physiological temperatures.

**NEW & NOTEWORTHY** We propose the interfacial water quantum-transition (IWQ) model to explain how proteins respond to temperature changes through specific quantum transitions of water at the protein-water interface. This model links key functional temperatures, such as human body temperature, to these transitions. By examining proteins like hemoglobin and thermosensitive channels, the IWQ model reveals a fundamental connection between water behavior and biological temperature regulation, shedding light on evolutionary adaptations in humans and animals.

body temperature; hemoglobin; protein-water interface; temperature; TRP channels

# INTRODUCTION

The body temperature of homeothermic species is kept constant within relatively narrow limits by the action of complex regulatory circuits involving thermal sensors and effectors. Despite countless man-years of research, the available body temperature data for homeothermic species, especially humans, remain experimentally determined values that are influenced by many factors (1-7). The actual body temperature varies depending on the circadian rhythm, measurement location, state of health, sex and ethnic origin of the subject, etc. (8-10). A meta-analysis of body temperatures recorded for 677,423 people, the oldest of whom was born ~200 years ago, showed that in the early nineteenth century the average body temperature of men was 0.59°C higher than it is today and during this period has decreased monotonically at 0.03°C per decade. For women, the decrease was virtually identical. This trend had been attributed to the improving average state of health of people (9, 10). It is obvious that this decrease cannot continue in a

linear fashion but must approach a threshold value, which may be approximated by the lowest body temperature measured in healthy subjects at rest (36.6°C for males). We refer to this threshold as the reference value of human body temperature. To be considered as such, it must be independent of the above influences: its nature must be determined by a physical mechanism. Such a physical mechanism that could establish reference temperatures for homeothermic species has not been found to date (11).

Erythrocytes [red blood cells (RBCs)] undergo striking shape changes in the bloodstream due to the prevailing flow forces, occurring within <100 ms (12). An incidental discovery by Artmann et al. in 1994 initiated the research on the subject of this article (13). If RBCs, with a resting diameter of 7.5–8.7  $\mu m$ , are aspirated in vitro into a micropipette with an inner diameter of 1.3  $\mu m$  at a negative pressure of -2.3 kPa (-17.25 mmHg), they block the orifice immediately after entering (14) up to a critical temperature  $T_C$  of 36.3  $\pm$  0.3°C. Above  $T_C$ , however, intact RBCs pass through the pipette with almost no resistance (15). This transition within  $\pm 0.3$ °C





is remarkably sharp, and its inflection point at 36.3°C is close to the lower threshold suggested for human body temperature (Fig. 1). This effect was quite a surprise to the RBC rheology and mechanics community (16-19).

Subsequent experiments conducted in the 30–44°C range, where an initial stage of structural perturbation was found to occur in hemoglobin (20, 21), aimed to understand the cause of the jumplike temperature transition of RBC passage. Our interdisciplinary effort involved a wide variety of methods, such as the micropipette aspiration technique (22), low-shear rotation viscometry (23), circular dichroism (CD) (21), and dynamic light scattering measurements (24, 25) as well as NMR spectroscopy (23) and various neutron scattering experiments on intact RBCs and hemoglobin samples (23, 26-28). In particular, CD measurements revealed that hemoglobin of all homeothermic species studied undergoes a partial and reversible thermal transition in the structural perturbation range with turning points, T<sub>C</sub>, close to the respective species' body temperatures (25). We concluded that hemoglobin acts as a molecular temperature sensor (23). Temperature transitions with T<sub>C</sub> between 36°C and 37°C were found with all experiments with human RBCs or hemoglobin, indicating that T<sub>C</sub> was neither a cellular nor an RBC membrane effect; moreover, it was independent of the pH of the buffer (range 6.8–7.8) and the calcium concentration (0– 18 mM) (22, 29). Intriguingly, temperature transitions were observed not only for oxy- and deoxy-hemoglobin but also for methemoglobin and even sickle cell hemoglobin (21) and thus appear to be inscribed into the globin architecture. In NMR T<sub>1</sub> measurements of highly concentrated RBCs in autologous blood plasma versus blood plasma alone, we found a transition at  $T_{C}\!\sim\!\!37^{\circ}\text{C}$  in both samples, but the temperature dependence of T<sub>1</sub> surprisingly showed opposite trends on either side of T<sub>C</sub> (see Fig. 3 in Ref. 23). Finally, micropipette passage experiments with human RBCs in deuterium oxide (D<sub>2</sub>O)-based buffer showed a passage jump at  $T_C = 37.2$ °C, i.e., 0.7°C higher than in H<sub>2</sub>O-based buffer (30, 31) (see Fig. 5

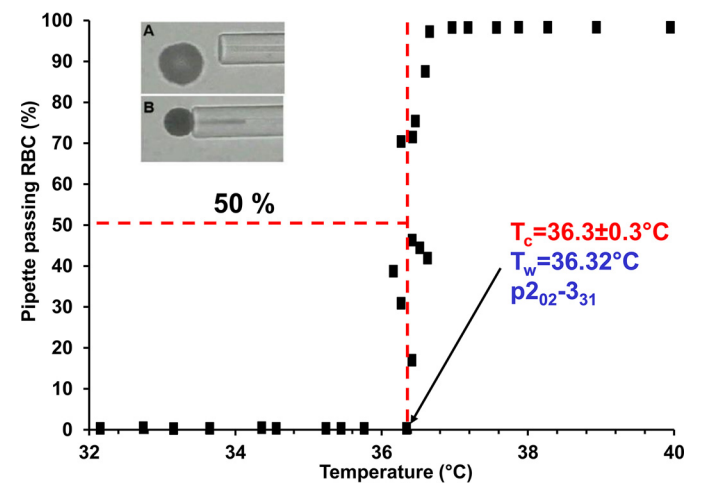


**Figure 1.** Micropipette red blood cell (RBC) passage experiment ( $n \sim 50$ RBCs per data point). Inset: pipette with inner diameter 1.3 µm; RBCs (dark), resting diameter  $\sim$ 8  $\mu$ m, before (A) and during (B) aspiration. Graph shows percentage of passing RBCs (squares); T<sub>C</sub>, measured critical passage transition temperature;  $T_W$  (blue), temperature of the triggering quantum-physical rotational transition of water with spectroscopic nomenclature (see below).

in Ref. 23), pointing to a role of the solvent "water" in this transition.

The body temperatures of homeothermic species are subject to evolution (8, 32-35). Indeed, the temperature transitions of hemoglobin are species specific (see Fig. 4 in Ref. 24) (25, 36). The RBC findings per se are mainly of interest to specialists; however, in-depth research into the physical nature of this phenomenon has led us to the fundamental concept that water is the key to understanding the observations. As a mechanism, we postulate that at the critical transition temperatures a molecular switch is triggered, which is based on the interaction of hemoglobin with water in the protein-water interface. This postulate does not require any specific assumptions about the structure of hemoglobin and should therefore be of general significance, i.e., be applicable to other proteins (22, 31, 37–39).

In homeothermic species, the hypothalamus is in charge of actively regulating body temperature (40). It obtains information on local temperatures in the organism via thermosensitive neurons with afferent cold and warm fibers (5, 41, 42). The actual temperature sensing, i.e., the conversion of the physical variable temperature into electrical signals, is carried out by membrane-spanning, temperature-sensitive cation channels that belong to the transient receptor potential (TRP) channel superfamily and feature exceptionally high temperature coefficients ( $Q_{10}$ ). Because of molecular adaptations, certain TRP channels are specifically "heat-activated" while others are "cold-activated." Although the precise molecular mechanisms governing temperature sensitivity are still largely unknown (43-49), there are numerous indications that the protein-water interaction in the water-exposed parts of TRP channels may play a key role (50-58). As is the case with hemoglobin, the temperature dependence of TRP channels is expected to differ from species to species (11).

In this work, we propose the interfacial water quantumtransition (IWQ) model as a novel paradigm for the explanation of temperature-dependent structural and functional transitions that occur at critical temperatures in proteins and other biomolecules. Its central postulate is that the experimentally measured transition temperatures, T<sub>C</sub>, are determined by quantum-physical reference temperatures, T<sub>w</sub>, relating to rotational transitions of temporarily free water molecules in the protein-water interface (59-64). After introducing the concept and explaining the transitions observed in RBCs and hemoglobin, we turn to membrane proteins, mainly thermosensitive TRP channels. Based on the rapidly growing body of knowledge on their structure and function, we use the IWQ model to justify the characteristic temperatures at which their thermal sensitivities switch between different  $Q_{10}$  regimes (45, 47, 49, 55, 56, 58, 65). Finally, we explain why the body temperatures, T<sub>B</sub>, of homeothermic species are always restored in the process of thermoregulation and do not drift on the temperature scale. Using previously unpublished data for human (mammalian) and chicken (avian) hemoglobin, we show that the abovementioned transition at the body temperatures of the respective species expresses itself as an inflection point in oxygen saturation. This suggests that the evolution of body temperatures in homeotherms may have been dominated by the optimization of critical physiological parameters in light of the interplay between available quantum-physical rotational

transitions of water at Tw on the one hand and the peculiarities of the protein interfacial structure on the other.

#### The Interfacial Water Quantum-Transition Model

# A thermally expanding, spherical model protein in aqueous solution.

Water is the most important solvent in biological systems and is fundamental to life (66-70). To set the stage for introduction of the interfacial water quantum-transition (IWO) model, we need to consider several important aspects of the anisotropic thermal expansion of a globular model protein (e.g., hemoglobin, myoglobin, serum albumin, immunoglobulins) in aqueous solution (71–73). In an aqueous, physiological environment, the majority of apolar amino acid residues are sequestered in the protein core because of their hydrophobicity and are not very dynamic. The mainly hydrophilic outer side chains form a protein-specific surface landscape and, together with the adjacent water, constitute the overall protein-water interface. The global thermal expansion coefficient of myoglobin crystals is  $115 \times 10^{-6} \, \text{K}^{-1}$ (between 255 K and 300 K); for liquid water it is  $70 \times 10^{-6}$  $K^{-1}$  (to compare and contrast, water ice 5  $\times$  10<sup>-6</sup>  $K^{-1}$ , glass  $8 \times 10^{-6} \,\mathrm{K}^{-1}$ ). Hence, myoglobin thermally expands about twice as much as bulk water (74). The thermal expansivity of proteins is subject to large variability and is highly anisotropic, which is essentially due to the influence of nonhydrated internal cavities, i.e., a variation in the density of internal van der Waals (vdW) interactions.

#### Topography and dynamics of the protein-water interface.

The distribution of hydrophilic and hydrophobic surface areas of the protein is temperature dependent because of the anisotropic thermal expansion of near-surface protein structures. As the thermal energy increases, secondary and tertiary protein structure elements tend to be destabilized, and distinct structural transitions can occur. The process is typically sigmoidal over temperature (20, 21). At the same time, the dynamics of the protein-water interface increases (75– 78). In polar surface areas, nonuniformly distributed hydrogen bonds form an irregular network between the protein and adjacent water. They bind and break continuously; only some are long-lived. In contrast, nonpolar, hydrophobic surface areas are covered by clusters of water molecules that are not hydrogen-bonded to the protein (Fig. 2), which have been termed cavity-wrap water (78, 81). The resulting topological profile is dynamic, with time constants according to Pal et al. (70) of 16-43 ps.

During thermal expansion, additional hydrophobic components are exposed on the protein surface, with ensuing changes in geometry and hydration (37, 82, 83). The transfer of bulk water to newly exposed (hydrophobic) surface areas requires inter alia an osmotic work of solvation, which contributes to the energetics of protein and solvent restructuring (26, 28, 37, 69, 84). The translational and rotational dynamics of water molecules is generally slowed down in the interfacial region because of hydrogen bonding with protein residues as well as volume exclusion effects. It seems plausible to assume that, particularly at hydrophobic sites devoid of hydrogen bonds between protein and water, the dynamics mismatch may result in temporary emergence of regions

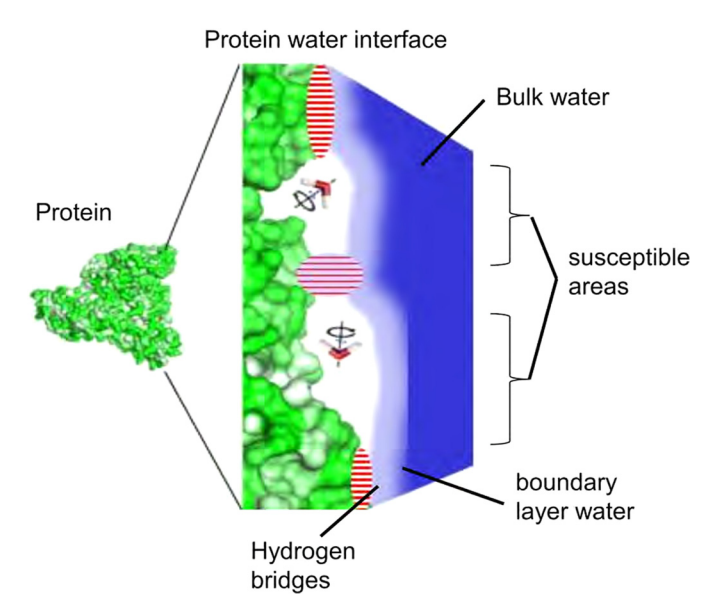


Figure 2. Topography of a protein-water interface. Left: surface representation of a generic protein. Right: close-up illustrating protein-solvent interactions. Hydrophilic surface regions are involved in protein-water H bonds with an irregular internal density (dashed red). In the hydration shell covering the surface area (light to dark blue), translational diffusion of water is restricted, and both density and order of hydration water are greater than those of bulk water. Hydrophobic surface areas ("susceptible" areas, see below), which may enlarge or newly arise during thermal expansion, are proposed as hot spots of rotational water transitions (79, 80).

with reduced density of solvent molecules. This intuitive view is supported by simulation studies investigating the dynamics of water in hydration layers. Unlike their hydrophilic counterparts, hydrophobic molecular surfaces are characterized by deviations from the Gaussian distribution of hydration water densities, featuring low-density tails. Indeed, the free energy required to form a solvent-free cavity  $(\Delta G_{cav})$  has been proposed as a generally applicable proxy to quantify hydrophobicity, even for surfaces as complex as those of proteins (Ref. 37 and references therein).

#### Rotational quantum transitions of free water molecules.

Water exists in two isomeric forms, as *para*-water (p-water) with the proton spin J = 0 and *ortho*-water (o-water) with J =1 (Fig. 3). In their unbound (gaslike) forms, both isomers undergo quantum-physical, molecular rotations involving distinct states that are described by quantum numbers (62, 64, 65, 85–89).

Transitions between rotational states occur by absorbing or releasing precisely defined quantum energies in the terahertz range of the electromagnetic spectrum (Fig. 3, Fig. 4). Because of the role of spin conservation, spontaneous transitions of p-water into o-water isomers and vice versa are quantum mechanically forbidden. An exception occurs when the energies of an o- and a p-level are close together (green dashed line in Fig. 4,  $\Delta E = 0.2 \text{ cm}^{-1}$ ).

Spin conversion is as well facilitated by the close proximity of some biologically important isotopes acting as catalysts. Its rate depends on catalysts' magnetic field gradient and density. Catalysts are for example triplet  $^{16}O_2$ ,  $^{57}Fe$  (2.1%, isotope fraction),  $^{39}K$  (44%),  $^{23}Na$  (100%),  $^{67}Zn$  (4%),  $^{25}Mg$  (10%),  $^{43}Ca$ (0.135%), <sup>13</sup>C (1.1%), and <sup>31</sup>P (100%) (91, 92).

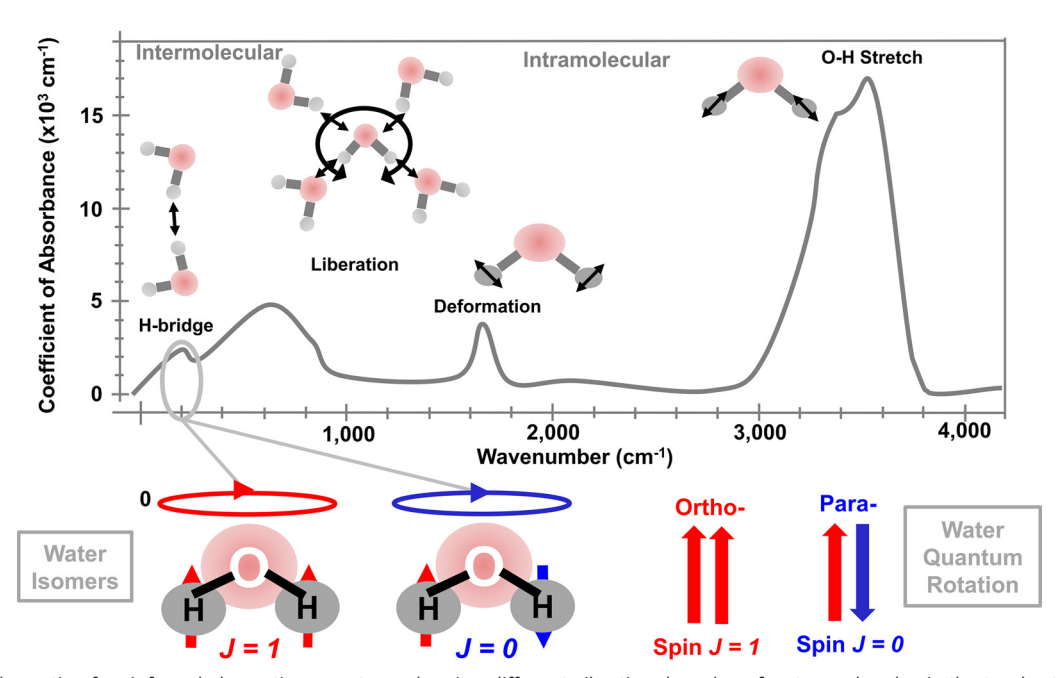


Figure 3. Top: schematic of an infrared absorption spectrum showing different vibrational modes of water molecules in the terahertz-infrared region. Marked (pink oval) is the energy range of the rotational transitions considered. Bottom: para (p)-water (nonmagnetic) with spin J = 0 and ortho (o)-water (magnetic) with spin J = 1.

In the past, the analysis of rotational spectra was largely limited to gases in which water molecules can rotate freely (Fig. 2) (60). Although an analogous situation can be generated by embedding water isomers in C<sub>60</sub> fullerene cages, in which they cannot form hydrogen bonds (93-97), rotational transitions are commonly thought to be suppressed in bulk water because of the extensive hydrogen bonding network (62, 98). This fundamentally correct view has been relativized by experiments using bidistilled liquid water (61, 63, 82, 99, 100) as well as DNA or protein solutions (64, 90, 101, 102) (discussed in Experimental evidence of rotational transitions in aqueous biopolymer solutions) but also by recent quantum mechanical molecular dynamics (MD) simulations. The latter highlight the statistical distribution in the density of hydrogen bonds in liquid water. In addition to the highly

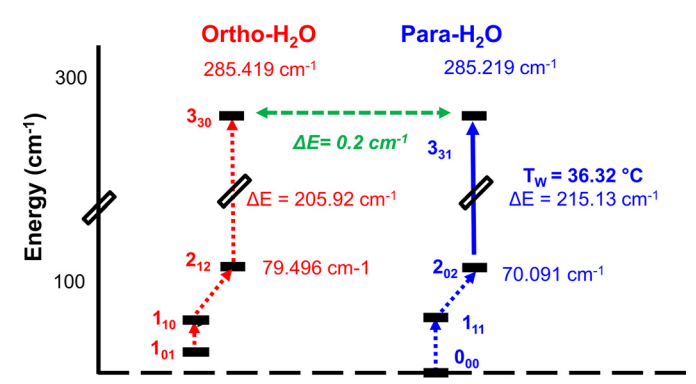


Figure 4. Excerpt from rotational quantum transition scheme of water isomers (85, 86, 90). The ground state energy of p-water (blue),  $pO_{00}$ , is zero; it does not rotate in this state, whereas the ground state energy of o-water,  $o1_{01}$ , is greater than zero. It always rotates (red).  $T_W$ , reference temperature. The energy differences between adjacent rotational quantum levels indicated by green  $(3_{31} - 3_{30})$ , red  $(2_{12} - 3_{30})$  or blue  $(2_{02} - 3_{31})$  arrows are referred to as  $\Delta E$ .

populated states (3 or 4 H bonds per water molecule), there are also states with lower coordination numbers. In fact,  $\sim$ 2% of all water molecules in pure water were found unbound at any given time, which would allow for shortlived quantum rotation without calling into question the fundamental statement on the extensive suppression of such transitions (82, 103). Moreover, the hydrogen-bonding network is well known to get more dynamic as temperature increases, with an anticipated growth of the fraction of instantaneously free water molecules. Adding to the fluctuations of hydrogen bonding density in bulk water, hydrophobic patches on solvated macromolecules are likely to constitute hot spots for water quantum rotation, because of the enhanced probability of low-density states favoring the occurrence of free water molecules (101). Effective hydrophobicity is assumed to be particularly prominent in high-curvature concave surface elements (80), suggesting that deep and narrow apolar cavities should provide the highest probability of vaporlike water. These considerations support the view that both in pure water and in the protein-water interface (Fig. 2) a small fraction of shortly "free" water molecules is available for rotational quantum transitions.

# Experimental evidence of rotational transitions in aqueous biopolymer solutions.

Rotational transitions in gaseous water can be detected with Raman spectroscopy and other classical methods of infrared spectroscopy (77). However, they are not well suited for resolving rotational transitions in liquid water or the protein-water interface with sufficient sensitivity because of the low proportion of usable signal, the unfavorable signal-tonoise ratio, and the considerable absorption of the water (61, 63, 100-102).

For the detection of rotational transitions in liquid water, significant progress has been made with coherent laser

spectroscopy methods. These methods are characterized by high spectral resolution and an excellent signal-to-noise ratio (61, 100, 104-107). This is due to the fact that the rotational spectra of the two water isomers are more dependent on the molecular mass than vibrational spectra, which are normally used to study molecular interactions in liquids (64, 102). With coherent laser spectroscopy, rotational transitions in pure liquid water as well as in aqueous solutions of DNA and protein have been demonstrated experimentally (101, 102, 108). It is important to note that the spectra of biomolecular solutions differ from those of pure water, confirming the notion that the protein or DNA surface provides sites that promote quantum transitions of the solvent. The peak amplitudes in their rotational spectra are a measure of the number of rotational transitions of free water molecules and their interaction with (susceptibility to) the electric field of two coherent laser beams at a given wave number. Peaks (resonances) appear in the spectrum at wave numbers  $\lambda^{-1}$ inducing rotational transitions in the sample volume (100, 106). In these experiments, the rotational spectrum of water isomers has thus emerged as a spectroscopic fingerprint of the dissolved biomolecule.

#### Mechanistic foundations of the IWQ model.

The local and temporary occurrence of free water molecules without H bonds in the protein-water interface is a fundamental premise of the IWQ model. In addition, given that the temperature of water (or any kind of matter) is directly related to the internal energy of its constituents, we adopt the view that rotational transitions can be initiated as characteristic resonance temperatures, T<sub>W</sub>, are reached (109, 110). Within the temperature range of protein structural perturbation, experiments often reveal transitions at critical temperatures, T<sub>C</sub>, at which protein functions or other properties change discontinuously (see below for examples). According to the IWQ model, these transitions can be explained by energy uptake of free water molecules in the protein-water interface (Fig. 2). These may undergo rotational quantum transitions by absorbing the discrete energy  $\Delta E_{n,m}$  that is defined by the rotational quantum states n and m, respectively. Assuming that such processes are initiated by collisions with thermal energy  $k \times T_W$  ties each transition to a characteristic rotational transition temperature T<sub>W</sub>:

$$\Delta E_{n, m} = h \cdot c \cdot \lambda^{-1} = k \cdot T_{W}(n, m)$$
 (1)

with h = Planck's constant, c = the speed of light, k = the speed of lightBoltzmann's constant, and  $\lambda^{-1}$  = the wave number (62, 109). All physically possible rotational transitions of free water involving quantum states of lower energy difference have already taken place before a specific Tw is reached, thus contributing to the energy landscape (79) of the protein surface below T<sub>w</sub>. At T<sub>w</sub> and above, however, absorption of higher quantum energies becomes possible, with effects determined by the actual number and distribution of free water molecules in the interface (Fig. 2). When the excited water molecules release their energy and reintegrate into the hydrogen-bonding network, this leads to local energy deposition at the protein-water interface. We propose the term "susceptible areas" for regions of the protein-water interface where rotational transitions are possible. At any given temperature, there may be several such areas, the size and distribution of which are protein specific (111, 112). If the water-mediated energy input at T<sub>W</sub> into these susceptible areas is sufficiently high, the protein can undergo local structural changes, thus attaining a new conformational equilibrium, which is often associated with a switch in protein function.

If the energy, often determined as enthalpy change  $\Delta H$ , taken up by the protein during a temperature-dependent transition at T<sub>C</sub> is known, the number of water molecules required to deliver this amount of energy via rotational transitions may be estimated from the quantum energies involved (85, 86):

$$N = \Delta H / \Delta E_{n, m} \tag{2}$$

As the temperature continues to increase, further rotational transitions are excited. Because of the changes in surface properties of the protein, at each rotational transition temperature a partially or completely different set of susceptible regions can be addressed, resulting in further conformational changes. The concept of susceptible surface areas applies not only to soluble proteins but also to membranespanning ones. Obviously, in these cases local energy accumulation via water quantum transitions is restricted to solvent-exposed regions or domains (Fig. 2; see Fig. 14 and Fig. 15).

The IWQ model postulates that, in the range of reversible perturbation, many pronounced temperature-dependent transitions in protein structure and function cannot be explained by continuous energy uptake of the protein-water system with rising temperature but require local energy input after a discrete water rotational transition temperature T<sub>W</sub> is reached. Thus, T<sub>W</sub> may represent the physically defined reference temperature of the protein transition observed at T<sub>C</sub>. Since T<sub>W</sub> is based on a quantum-physical property of water molecules, it is independent of solution pH, chemical potential, salt concentration, and other proteins in the aqueous environment.

What happens as the temperature decreases? When the temperature drops below T<sub>W</sub>, the energy introduced into the local protein interface regions is recovered. In the structural perturbation stage, IWQ transitions should be reversible, unless this is hindered by secondary reactions, such as protein aggregation (21, 23, 78) or semipermanent thermal denaturation, as with some temperature-sensitive TRP channels (113, 114).

# Application of the IWQ Model to Human RBCs and Hemoglobin

# Temperature transition of RBC passage through micropipettes (RBC passage transition).

The cytosol of RBCs is mainly comprised of freely suspended, almost spherical Hb molecules that form a crowded medium (27, 115–117). It exhibits a Newtonian flow behavior at physiological concentration (12). The relaxation times of RBCs, which are determined not only by the cell membrane viscosity but also by the viscosity of the cytosol, decrease linearly and monotonically with increasing temperature up to  $\sim 40^{\circ}$ C (19, 118). In particular, it does not show anomalies around human body temperature (119-121).

In contrast, passage experiments with RBCs suspended in phosphate-buffered saline through 1.3-µm micropipettes at a high aspiration pressure of -2.3 kPa revealed a very sharp and highly reproducible temperature transition

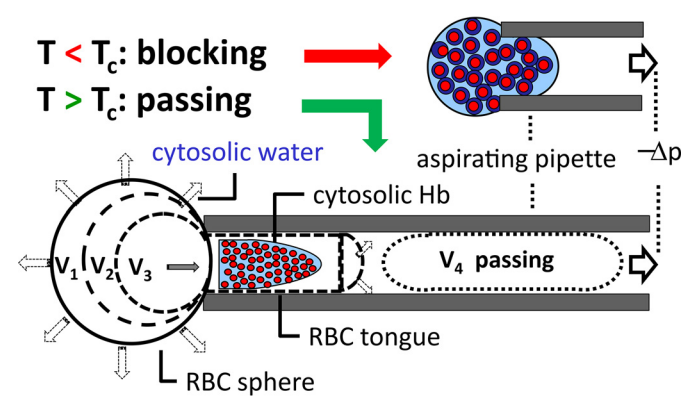


Figure 5. Red blood cell (RBC) passage transition: Human RBCs in a micropipette undergo a steplike transition at the critical temperature  $T_C$  $36.3\pm0.3^{\circ}\text{C}.$  During the entry process, the Hb solution in the RBC cytosol is mechanically sheared. Simultaneously, water is displaced from the cytosol, reducing the volume of the outer RBC sphere. Inside the sphere, Hb forms a highly concentrated, viscous Hb gel. At T<sub>C</sub>, its viscosity undergoes a phase transition, allowing the whole RBC to pass the pipette. At T > 37 $^{\circ}$ C, the pipette does not cause any significant resistance to the RBC passage. V, RBC partial volume;  $\Delta p$ , aspiration negative pressure in the pipette.

in the passageability (RBC passage transition) at  $T_C$  =  $36.3 \pm 0.3$ °C (Fig. 1). Below T<sub>C</sub>, the RBCs block the pipette, while the Hb concentration in the spherical RBC trail remaining outside the pipette increases to 50 g/dL (Fig. 5) (13). From  $\sim$ 37°C onward, however, they pass through unhindered (15).

Applying the IWO model, we postulate that this is the result of quantum mechanical rotational transitions in the Hb-water interface at  $T_W = 36.32^{\circ}\text{C}$  (p2<sub>02</sub>-3<sub>31</sub>). This transition causes a sudden drop in cytosolic fluidity. Within the accuracy of the measurement, the temperatures  $T_{\text{\scriptsize C}}$  and  $T_{\text{\scriptsize W}}$  can be considered identical; moreover, they correspond to the average body temperature of a healthy person,  $T_B = 36.6$ °C (99% range 35.3–37.7°C) (107) and thus might actually represent the basal limit of the human body temperature.

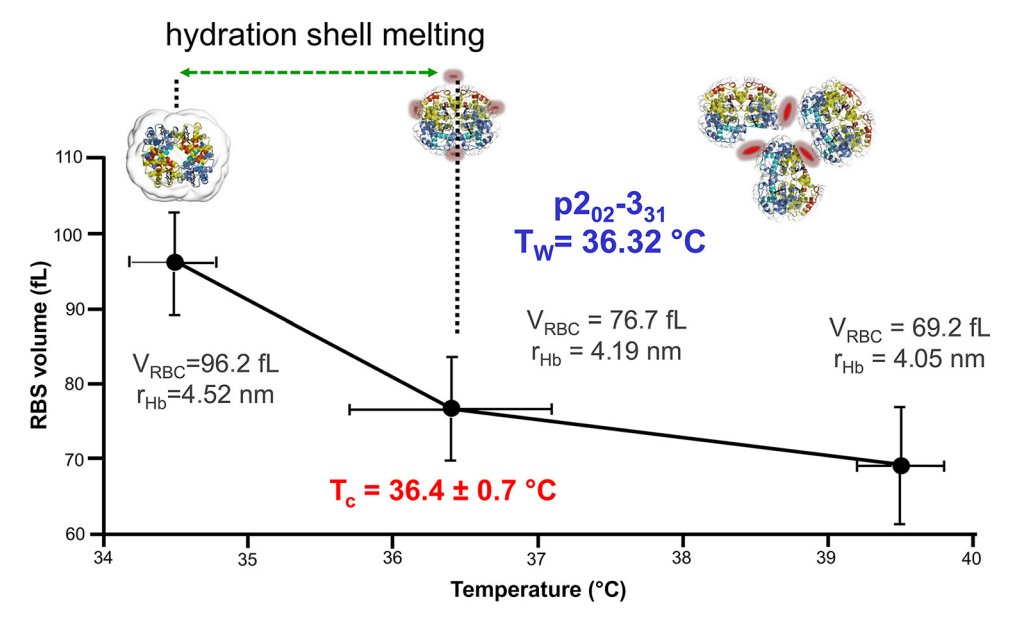
To test whether the isotopic state of the hydrogen in the water molecule has an influence on the RBC passage transition, micropipette experiments were performed with RBCs suspended in phosphate buffer containing deuterium oxide (D<sub>2</sub>O) instead of H<sub>2</sub>O. Deuterium-based hydrogen bonds are slightly stronger than protium-based ones because of the difference in mass between deuterium (D) and protium (H), implying a higher stability of protein-solvent and solvent-solvent interactions. Thus, it was expected that the critical transition temperature should be shifted to higher values, which we indeed observed. The critical transition temperature for RBC passage was  $T_C$  ( $D_2O$ ) = 37.2°C, corresponding to an upward shift by 0.8°C. In accordance with the IWQ model, we assign this inflection point to the rotational transition p982-991 with  $T_W = 37.09$ °C (see Fig. 5 in Ref. 23).

# Temperature transition of RBCs trapped in micropipette orifices (RBC volume transition).

With the same negative pressure in the pipette as above, but a smaller internal diameter of 1.1  $\mu$ m, at which no RBC can pass through, the temperature dependence of the equilibrium RBC volume,  $\Delta V/\Delta T$ , between 34.5°C and 39.5°C was measured (23) (Fig. 6). Since the RBC membrane remains intact during pipetting, the aspiration force causes an increase in cytosolic pressure.

Consequently, the cytosolic bulk water is squeezed out through the aquaporin channels (66) until an equilibrium is reached, which is presumably dictated by the amount of water tightly bound by hemoglobin, the major colloid osmotic agent in the RBC cytosol. The observed decrease in RBC volume with increasing temperature can thus be attributed to the conversion of Hb-bound water to bulk water (23). In other words, in this temperature interval, the Hb hydration shell "melts" and bound water becomes bulk water. At  $T_C$  = 36.4 ± 0.7°C an inflection point of the equilibrium RBC volume was found (RBC volume transition), again coinciding with the rotational transition  $p2_{02}$ - $3_{31}$  at  $T_W = 36.32$ °C. The volume loss with temperature ( $\Delta V/\Delta T$ ) was quite steep at T < $T_C$  (-10.3 fL/°C) but flattened to -2.4 fL/°C above  $T_C$ , indicating that the melting process of Hb-bound water is essentially complete at  $T_C = T_W$ . As further indirect evidence for the loss

Figure 6. Red blood cell (RBC) volume transition. Individual RBC volume (V<sub>RBC</sub>) as a function of temperature is shown. For each temperature step, 12 individual RBCs were aspirated (n = 12). Single-RBC volume was calculated from microscopic images. The abbreviation r<sub>Hb</sub> stands for the estimated radius of the hemoglobin molecules in the spherical outer part of the aspirated RBC. It is calculated from the micropipette data and the physiological intracellular Hb concentrations. At critical temperature  $T_C=36.4\pm0.7^{\circ}C,$  there was a significant kink. Below T<sub>C</sub>, the volume loss slope was 4.2 times higher than above. Apparently, water "melted" from the Hb hydration shell at a given temperature into bulk water is expelled from the cytosol. At temperatures above the transition point, a proportion of water molecules remain bound to the Hb surface forming a hydration shell. Used with permission from Artmann et al. (23).



of water bound to Hb below T<sub>C</sub>, we note that in NMR measurements on plasma-suspended RBCs the T<sub>1</sub> relaxation time increases in this temperature range but remains almost constant above the transition temperature (see Fig. 5 in Ref. 23). It is crucial to understand that the RBC volume transition is physically distinct from the RBC passage transition. Whereas the former is a stationary phenomenon, the latter is a fluiddynamic effect in which shear forces act.

Estimates showed that the applied thermal energy is too small to explain the inflection points of the two pipette experiments (Fig. 5 and Fig. 6). The small difference in colloidal osmotic pressure of the cytosol in the selected temperature range cannot have caused the transition either (22). Thus, in our opinion, classical physicochemical theories are unable to explain the occurrence of the observed inflection points. Together with temperature-dependent dynamic light scattering experiments (24, 25) and Hb-solution viscosity recordings (Fig. 7; Ref. 13) the above data support the view that the rotational transition of water at T<sub>C</sub> leads to a sudden increase in hydrophobicity of the Hb surface, enabling lowfriction sliding of the Hb molecules and hence the RBC passage transition with the 1.3-µm pipette. Note that we are referring to an effective hydrophobicity, which cannot simply be deduced from the fraction of apolar moieties exposed on the protein surface. In fact, the numerous solvent-accessible side chain and main chain atoms featuring different polarity cooperate in complex and nontrivial ways, depending on their relative arrangement, to yield local and global patterns of hydration (37, 80, 122). Consequently, a moderate rearrangement of a given set of protein surface elements may be sufficient to alter solvent interaction, and even though an increase in temperature may be expected to result in partial unfolding and hence exposure of additional apolar side chains, the effect on global hydrophobicity may be disproportionate. The mechanism we are proposing for the RBC passage transition differs fundamentally from a previously expressed view (110).

The narrower 1.1-µm pipettes (Fig. 6) do not allow for any RBC passage but uncover a release of bound water to the bulk of the cytosol, which precedes the actual transition at T<sub>C</sub>. The intriguing observation that melting of the hydration layer ends (within the precision of the experiment) at the transition temperature, T<sub>C</sub>, suggests that the loss of hydration water may sensitize the protein to the energy uptake by quantum absorption, e.g., by altering the dynamics of surface-exposed residues, which has been observed as well in neutron scattering experiments (see Fig. 5 in Ref. 26).

#### Temperature transitions of Hb solutions in a rotary viscometer (Hb viscosity transition).

To rule out RBC-membrane-related switches, such as a sudden loss of adhesion between the RBC membrane and the inner surface of the pipette or a sudden change in the water permeability of the aquaporins, as causes of the RBC transitions described, concentrated Hb solutions were analyzed with a rotational viscometer at a shear rate of  $5.89 \text{ s}^{-1}$ . The equilibrium time between successive temperature steps was 15 min. Hb concentrations were chosen that occur in the RBC sphere (Fig. 1) during the micropipette RBC passage (13, 22, 29) (Fig. 7). Considering the IWQ model, the observed transition at  $T_C = 36.4^{\circ}\text{C}$  is caused by rotational transitions  $p2_{02}$ - $3_{31}$  of free water molecules at the Hb-water interface. At  $\sim$ 37°C, a stall occurs, which leads to the observed independence of the viscosity of the Hb solution from the concentration at elevated Hb. The viscosity range between 36.4 and 37°C represents a transition state.

It is important for the comparison and interpretation of the data that fluid dynamic shear forces act in the cytosol or in the Hb solution in both micropipetting experiments (Fig. 5) and rotational viscometry (Fig. 7). In contrast to viscometry, however, in the pipette experiments cellular water is expelled into the extracellular space at the same time. The total volume of the RBC is reduced, which implies that the average water content per molecule of Hb is also reduced.

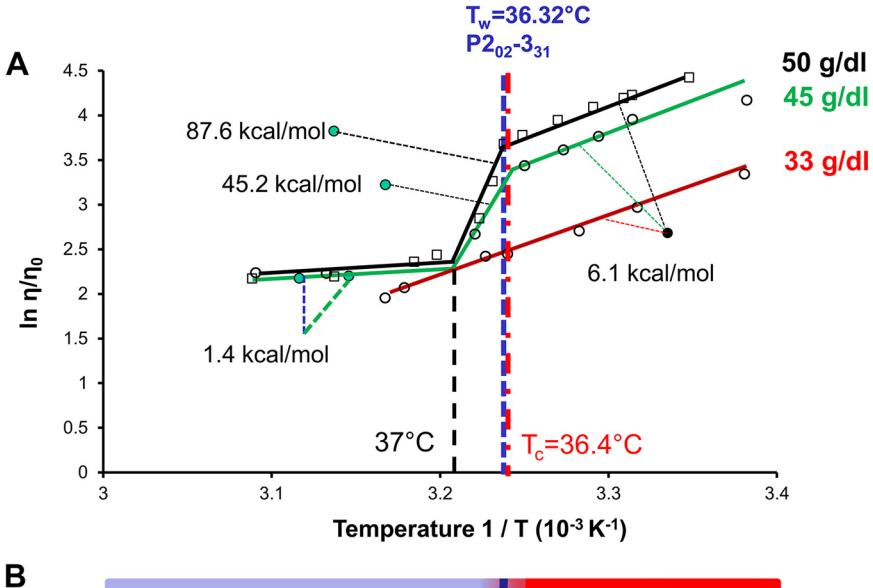


Figure 7. Hemoglobin viscosity transition: Arrhenius plot of the relative viscosity  $[ln(\eta/\eta_0)]$  of concentrated human hemoglobin (n = 10 per data point). A: at 33 g/dL, the viscosity decreases monotonically with increasing temperature. No temperature transition was seen. At 45 and 50 g/dL, however, a transition became visible at critical temperature  $T_C =$ 36.4 ± 0.3 °C corresponding to the interfacial water quantum (IWQ) transition p2<sub>02</sub>-3<sub>31</sub> at reference temperature  $(T_W) = 36.32^{\circ}C$ . The relative viscosity is concentration dependent at temperatures below T<sub>C</sub>. From T  $\sim$ 37°C on, there was no difference between the 2 higher concentrations within measurement accuracy. B: the viscosity transition of hemoglobin (Hb) is attributed to a sudden change in effective hydrophobicity at the Hb surface. Used with permission from Artmann et al. (13).

Hydrophilic

The Hb concentration in the RBC's globular part remaining outside the pipette increases up to 50 g/dL below  $T_C$  =  $36.4 \pm 0.3$ °C (13, 23, 123). Our observation of hydration water melting off Hb in RBCs as a function of temperature must also hold in the viscometer, but unlike in RBCs under aspiration stress the average water content per Hb molecule remains constant (22).

The relative viscosity,  $ln(\eta/\eta_0)$ , in the Arrhenius plot decreased monotonically and linearly with 1/T between 23°C and 42°C for the 33 g/dL Hb solution. There was no inflection point. In contrast, at Hb concentrations of 45 and 50 g/dL, an abrupt and significant temperature transition in Hb relative viscosity was observed at  $T_C = 36.4^{\circ}C$  (Hb viscosity transition) (Fig. 7). Up to T<sub>C</sub>, Hb solution viscosity was concentration dependent, in agreement with expectation and with published data (120). The ratio of free bulk water molecules,  $N_{free}$ , to hemoglobin-bound water molecules,  $N_{bound}$ , at T  ${\sim}25^{\circ}C$ and concentrations of 33 g/dL, 45 g/dL, and 50 g/dL is estimated to be  $N_{free}/N_{bound} = 5.3$ , 3.0, and 2.0, respectively, corresponding to approximately seven, four, and three molecule layers of free bulk water between adjacent Hb molecules (22). Despite these differences, the Arrhenius plot yields the same apparent activation energy, within the accuracy of the measurement, in all three cases (6.1 kcal/mol). Intriguingly, the Hb viscosity transition is only observed when the translational diffusion is severely restricted because of the close proximity of the Hb molecules. The jump in activation energy at  $T_C = 36.4$ °C amounts to  $\Delta E_a = 45.2$ –6.1 kcal/mol = 39.4 kcal/mol at 45 g/dL and to  $\Delta E_a = 87.6-6.1$  kcal/mol = 81.5 kcal/mol at 50 g/dL. At  $\sim$ 37°C the temperature dependence of relative viscosity changes again for the higher Hb concentrations, switching to an apparent activation energy of only 1.4 kcal/mol; this corresponds to a difference  $\Delta E_a = 1.4-6.1$  kcal/ mol = -4.7 kcal/mol w.r.t. the low-temperature regime.

Applying the IWQ model, we propose the increase in Hb hydrophobicity resulting from water quantum absorption at  $T_W = 36.32$ °C to trigger a fluid dynamic instability (124) in concentrated Hb solutions. The first hydration shell in the Hb interface contains  $\sim$ 2,300 water molecules as reported by Stadler et al. (27). Since the energy absorption of the

rotational transition of a water molecule at  $p2_{02}$ - $3_{31}$  is known, the percentage of water molecules that are required to provide the energy for the viscosity jump can be estimated from the total energy taken up by the Hb molecule including its hydration shell. Taking the activation energy differences mentioned above as a proxy yields numbers of 64 and 133 (Eq. 1 and Eq. 2) for the transitions at 45 and 50 g/dL, respectively, amounting to only 2.8% and 5.8% of the water molecules of the first hydration shell.

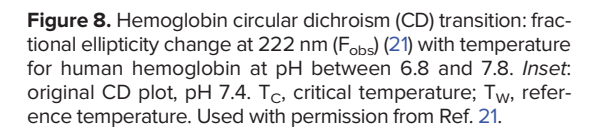
The ultimate cause of these temperature transitions is water. Even after calcium-induced cross-linking of cytosolic hemoglobin in RBCs or hemoglobin in solution, we found a temperature transition at a critical temperature T<sub>C</sub> =  $36.4 \pm 0.3$ °C (22, 29), which again coincides with  $T_W =$  $36.32^{\circ}$ C of the rotational transition p2<sub>02</sub>-3<sub>31</sub>. This means that the position of T<sub>C</sub> on the temperature scale remained unchanged even after significant alteration of protein-protein interactions. As expected, calcium did have strong effects on RBC passage through micropipettes and Hb suspension viscosity, confirming that environmental factors influence the biological effects induced by rotational transitions of water. The transitions themselves, however, always take place at the same temperatures, which are predetermined by quantum physics.

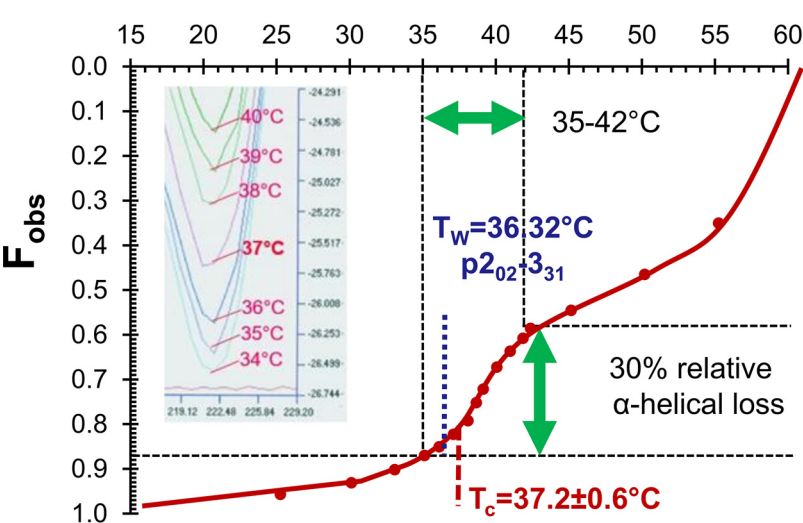
#### Hemoglobin solution circular dichroism (Hb CD transition).

In the temperature range between 35°C and 39°C, CD measurements with human hemoglobin showed a transition in ellipticity at 222 nm, indicating an accelerated decrease in  $\alpha$ -helix content (125). Independent measurements on different CD instruments resulted in transition temperatures of  $T_C = 37.2 \pm 0.6^{\circ}C$  (21),  $T_C = 37.1 \pm 0.5^{\circ}C$  (25), and  $T_C =$  $36.5 \pm 0.5$ °C (24). We attribute the varying T<sub>C</sub> to systematic deviations of the actual temperature in the sample volume from the temperature set on the device. As reported by Artmann et al. (21), the CD transition is independent of Hb oxygenation, pH, and other factors (Fig. 8).

We assign the rotational transition p2<sub>02</sub>-3<sub>31</sub> of water at  $T_W = 36.32^{\circ}C$  to these critical temperatures. In accordance

Temperature (°C)





with the IWQ model and our conclusions for other Hbrelated transitions, this accelerated decrease in  $\alpha$ -helix content correlates with an increase in Hb surface hydrophobicity. This can be inferred from independent dynamic light scattering measurements on human Hb revealing  $T_C =$  $36.4\pm0.8^{\circ}\text{C}$  (25) and  $T_{C}=36.5\pm0.5^{\circ}\text{C}$  (24). Above these  $T_{C}s,$ the aggregation of Hb increases at a significantly elevated slope. The CD transition is therefore likely to be based on the same quantum mechanical mechanism as the RBC passage and the Hb viscosity (23) transitions, with additional hydrophobic patches forming abruptly at Tw. Tw thus separates two different physical states of the Hb surface on the temperature scale (Fig. 2) (20, 37, 67, 126, 127).

#### Hemoglobin crystal thermal transitions (Hb crystal transition).

Water is a ubiquitous component of protein crystals, typically amounting to 30-70% of total crystal volume. Gevorkian et al. (128, 129) grew monoclinic crystals of human oxyhemoglobin and measured the dynamic Young modulus (modulus of elasticity) E as a function of temperature between 25 and 50°C. Intriguingly, it changed abruptly at several transition temperatures and remained constant in between (Fig. 9).

The strength of lattice interactions, and hence the Young modulus, depends on the ambient humidity of the crystal, with E being  $\sim$ 8 times larger at 75% relative humidity than at 95%; the crystal becomes softer because of water absorption (129). Similar experiments have been reported for lysozyme crystals (130). It is interesting that the Young modulus increases abruptly at  $T_W = 25.93^{\circ}$ C, whereas it decreases successively at all higher transition temperatures. Conceptually, a protein crystal can be regarded as an extremely concentrated protein solution, in which positions and orientations of individual molecules are restrained by lattice contacts

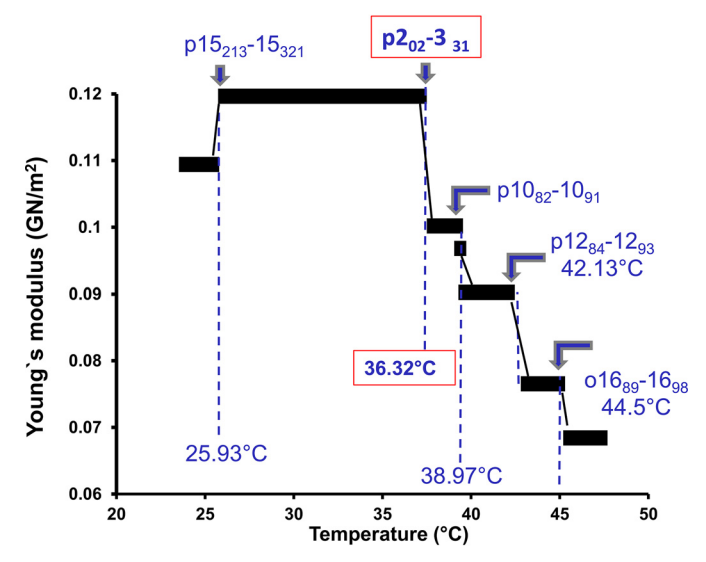


Figure 9. Hemoglobin crystal transition: temperature profile of the Young modulus E of human oxyhemoglobin crystals measured with an oscillating 2-plate system (~5 kHz). E changes in sharp steps and remains constant in between. At  $T > 49^{\circ}C$  crystals clove to pieces. Interfacial water quantum (IWQ) transitions and their characteristic temperatures T<sub>W</sub> (blue) are assigned to observed critical temperatures T<sub>C</sub>. Used with permission from Ref. 129.

while the majority of hydration water is preserved. We postulate that the increase in the Young modulus at  $T_W = 25.93^{\circ}C$ (p15<sub>312</sub>-15<sub>213</sub>) results from an abrupt change in the hydrogen bonding architecture at the protein-water interface and/or moderate alterations of the protein surface affecting crystal lattice contacts. Obviously, structural alterations must be moderate enough to not disrupt the lattice contacts, especially since nonfixated crystals were used in these studies. An increased density of hydrogen bonds, or other noncovalent interactions, would explain the observation of the crystal becoming less elastic (37, 95, 131). The new binding state is maintained from  $T \ge 25.93^{\circ}C$  until changing to another H-bridge arrangement at  $T_W = 36.32^{\circ}C$  (p2<sub>02</sub>-3<sub>31</sub>). At  $T_W =$ 36.32°C, the crystal suddenly "softens." Note that the resonance method applied here for measuring the Young modulus generates shear forces (91) between Hb molecules and adjacent water layers. We hypothesize that, analogous to the viscosity transition described above, an increase in the effective hydrophobicity of Hb due to rotational transitions of water in the protein-water interface leads to a decrease in the density of protein-water hydrogen bonds. This might enable the onset of low-friction sliding, rationalizing the sudden drop of the Young modulus.

In the range between  $T_W = 25.93^{\circ}C$  and  $T_W = 36.32^{\circ}C$  further rotational transitions are expected, but these do not appear to have any effect on the Young modulus, either because the energy input is too small to cause a change or because the alterations are silent w.r.t. crystal elasticity.

# Colloid osmotic pressure of RBCs in autologous plasma (Hb-COP transition).

In a series of in vitro experiments, we measured the colloid osmotic pressure (COP) of human RBCs resuspended in autologous plasma with an average RBC content of  $77.6 \pm 5.3\%$  by volume (RBC-in-plasma sample) versus autologous plasma alone (plasma sample) at  $29^{\circ}$ C  $\leq$  T  $\leq$  39.5 $^{\circ}$ C (see Fig. 4 in Ref. 23). This was to elucidate as closely as possible the in vivo environment of the hemoglobin-water interaction inside RBCs (23, 120). The COP of both samples increases linearly and parallelly with temperature, with the plasma sample COP consistently 0.27 kPa higher. It is reasonable to assume that this is due to a small proportion of plasma proteins adhering to the RBC surfaces in the RBC-plasma sample, thus reducing the free plasma protein concentration and its COP. Although the COP of the plasma sample continued to increase linearly with temperature, the parallelism of the COPs ended at  $T_C = 37.1 \pm 0.2^{\circ}$ C. From there on, the COP of the RBC-plasma sample decreased rapidly, at 39.5°C being 0.73 kPa lower than that of the plasma sample. Our assumption is that from T<sub>C</sub> upward cytosolic water leaks from the RBC into the surrounding plasma. This dilution effect causes the plasma protein concentration to decrease and the total COP to decline in parallel. Based on the IWQ model, the transition at T<sub>C</sub> induces partial hydrophobization on the Hb surfaces, triggering cytosolic Hb aggregation and thus reducing the number of colloid osmotically active particles. As a result, cytosolic water is released into the extracellular space (27, 31, 99, 132, 133).

The Hb-COP transition takes place in the full absence of fluid dynamic shear forces. Taking into account the above considerations and the technical shortcomings of T<sub>C</sub> measurement, we hypothesize that the COP transition is another manifestation of IWQ transition p2<sub>02</sub>-3<sub>31</sub> with characteristic temperature  $T_W = 36.32^{\circ}$ C, proposed above as a reference for basal human body temperature  $T_{B,human}$ . The release of water from the cytosol of RBCs may represent a contribution to homeostasis during fever in humans (40, 46, 134). From the COP data, it can be estimated that an adult with a fever temperature of 39.5°C transfers ~500 mL of water from RBCs into the blood plasma, partially compensating for the loss of sweat water (23). Analogously, we assume that additional water is recruited from muscle cells during fever because of aggregation of myoglobin setting on possibly as well at  $T_C$  (134, 135). A possible physiological relationship between the release of water by the RBCs from  $T_W = 36.32^{\circ}C$ on and the increase in the rate of skin temperature-related sweating (4) as the core body temperature exceeds ~36.5°C is only hinted at here.

#### **IWQ Transitions of Thermosensitive TRP Transmembrane Channels**

#### Neuron thermal sensitivity.

Using the local temperature distribution in an organism for regulation of its body temperature requires sophisticated biological sensing mechanisms (45, 49, 54, 136). First, a neuronal temperature transition on the organ level is discussed here (42). The study involved the stimulation of heat-sensitive splanchnic nerves in the dorsal wall of the abdominal cavity of rabbits through the perfusion of thermodes with water at temperatures ranging from 12°C to 50°C. Up to a critical temperature,  $T_C \sim 36-38^{\circ}C$ , neural afferent activity remains constant. It then changes to an almost linear increase with temperature (see Fig. 3 in Ref. 42). Applying the IWQ model, the rectal body temperature of the rabbit  $T_B$  $\sim$ 38.4 ± 0.6 °C can be assigned the IWQ reference temperature  $T_W = 38.69$ °C (o12<sub>012</sub>-12<sub>111</sub>). Thus, the authors provide a (rare) example of a critical switching temperature at the organ level,  $T_{C,organ}$  (39, 42, 61, 137, 138). It seems reasonable to assume that such higher-order switching temperatures are intrinsically related to the critical temperatures, T<sub>C</sub>, of key molecular temperature sensors, in this case the heat-sensitive TRP ion channels. These include the noxious heat-sensitive TRPV1 (VR1) channel (139, 140) as well as the warmsensitive TRPV3 channel (141) (discussed below).

A further example is the temperature profile of the action potential frequency recorded from individual thermosensitive neuronal fibers, the cold fibers (A $\delta$  fibers) and the warm fibers (C fibers), after thermal stimulation of cat tongue nerves (Fig. 10) (14, 31, 41, 44, 142).

The cold-sensitive A $\delta$  fibers clearly show multiple regions of different temperature sensitivity (143). The starting point of continuous discharge correlates with  $T_{\rm W}=12.19^{\circ}C$ (p873-893). There is an intermediate minimum and a maximum located close to  $T_W = 15.6$  °C (p13<sub>77</sub>-13<sub>86</sub>) and  $T_W =$ 26.71°C (o4<sub>23</sub>-5<sub>32</sub>), respectively. The activity stops around  $T_W = 36.32^{\circ}$ C (p2<sub>02</sub>-3<sub>31</sub>). Interestingly, a second temperaturesensitive range sets on at  $\sim T_W = 45.74^{\circ} \text{C} (04_{14} - 5_{23}) (144)$ . We recognize an analogy to the "cold sensation paradox" that is typically observed in humans at temperatures above 45°C. The warm-sensitive C fibers instead begin firing at  $\sim\!\!T_W=$  $18.75^{\circ}$ C (p3<sub>31</sub>-4<sub>40</sub>) and reach a maximum rate close to T<sub>W</sub> =

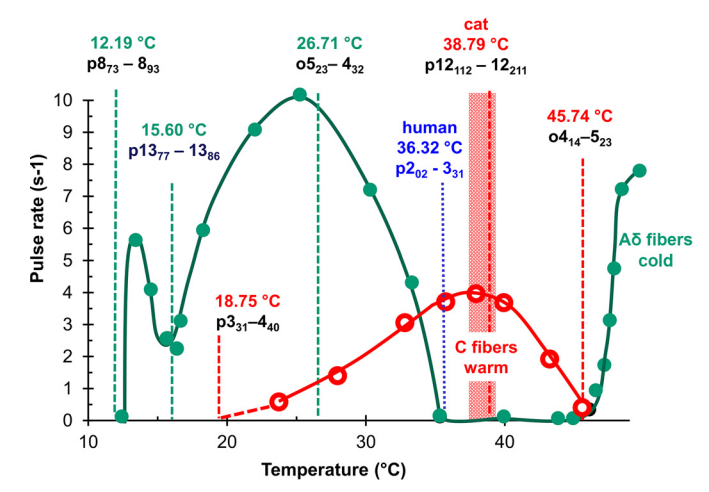


Figure 10. Temperature-sensitive neurons (cat): steady-state firing rate of individual cold-sensitive A $\delta$  fibers (green) and warm-sensitive C fibers (red) after thermal stimulation of the lingual nerve of cats at constant temperatures between 10 and 50°C. The normal body temperature range of cats is shaded red. Temperatures at which the sensitivity of the 2 fiber types is turned on, turned off, or turned over are assigned interfacial water quantum transition (IWQ) reference temperatures. Used with permission from Ref. 41.

38.79°C (p12<sub>112</sub>-12<sub>211</sub>), which is within the cat's normal body temperature range,  $T_B \sim 38.3 - 39.2$ °C. Sensitivity dissipates at  $T_W = 45.74$ °C ( $o4_{14}$ - $5_{23}$ ), the same temperature at which the cold-sensitive  $A\delta$  fibers resume their temperature sensitivity. In generating afferent temperature signals over the entire temperature range, C and Aδ fibers complement each other (138, 145, 146).

# Temperature-sensing TRP channels.

The TRP channels TRPM8 (cold sensor), TRPV3 (warm sensor), and TRPV1 (noxious heat sensor) are molecular temperature sensors with exceptionally high Q<sub>10</sub> values in certain temperature ranges (14, 43, 45, 47, 50, 51, 54, 57, 58, 65, 93, 136, 140, 147).

The cold-sensitive TRPM8 is expressed in ~15% of small dorsal root ganglion neurons and is activated below  $T_C =$ 25°C (Fig. 11) (143). Whole cell patch-clamp data obtained with HEK293 cells showed robust temperature-activated

Channel activation is usually described using a two-state model, i.e., under the simplified assumption of a single open and closed state, respectively. Figure 11 displays a Van 't Hoff plot of the equilibrium constant  $K_{eq} = [\text{open}]/[\text{closed}]$ . The plot exhibits several regions of differential temperature dependence (Q<sub>10</sub>), with linear segments separated by inflection points at  $T_C = 10^{\circ}$ C,  $18^{\circ}$ C, and  $25^{\circ}$ C. Assigned IWQ reference temperatures are indicated. At  $T_C = 18^{\circ}C$  the enthalpy and entropy of channel opening (related to slope and intercept of the linear fit) change by  $\Delta\Delta H = 52 \text{ kcal mol}^{-1}$  and  $\Delta\Delta S = 174 \text{ cal mol}^{-1} \text{ K}^{-1}$ . Based on the IWQ model, the energy required for the underlying structural perturbation is covered by rotational transitions of water at  $T_W = 18.43^{\circ}$ C (o3<sub>30</sub>- $4_{41}$ ). At this  $T_{W}$ , one water molecule absorbs an energy of 0.58 kcal/mol (wave number of 202.69 cm<sup>-1</sup>). The change in gating enthalpy at  $T_C = 18^{\circ}C$  corresponds to  $\sim 90$  rotational transitions of water molecules per tetramer (*Eq. 1* and *Eq. 2*). Since the channel is composed of four identical subunits, the

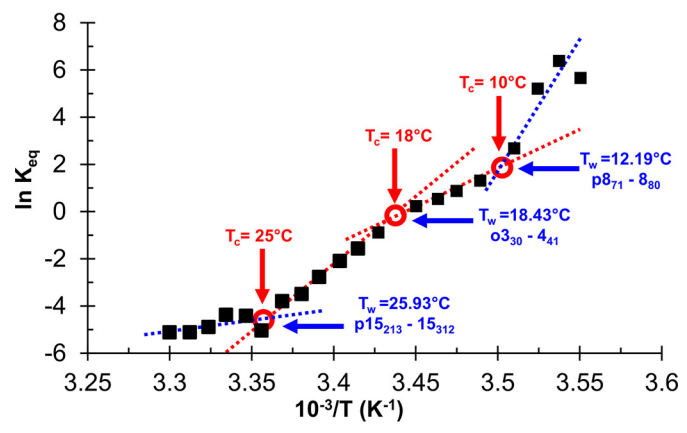


Figure 11. Cold sensitive TRPM8: Van 't Hoff plot of steady-state membrane channel activity,  $K_{\rm eq}$ , measured by whole cell patch-clamping at 60 mV holding potential. The authors performed a linear regression analysis for 2 temperature regimes (red dotted lines),  $10^{\circ}$ C to  $18^{\circ}$ C ( $Q_{10} = 3.3$ ) and  $18^{\circ}$ C to  $25^{\circ}$ C ( $Q_{10} = 23.8$ ). However, we identify 2 more regimes, one at  $T < 10^{\circ} C$  and another shallow one at  $T > 25^{\circ} C$  (blue dotted lines). The 3 critical temperatures  $T_{\text{C}}$  were assigned to interfacial water quantum transition (IWQ) reference temperatures  $T_W$ . Deviations between  $T_W$  and  $T_C$ reflect experimental temperature uncertainties. Used with permission from Ref. 143. Copyright (2004) National Academy of Sciences.

changes to protein conformation should be statistically symmetric, and further synchronization may occur via allosteric coupling. For TRPM8, two additional enthalpy jumps were observed at  $T_C = 25^{\circ}C$  and  $T_C = 10^{\circ}C$ . Above 25°C, the TRPM8 channel follows a shallower phase at very low activity. Below  $T_C = 10^{\circ}$ C, the authors described the regime as "saturated," but the data may indicate a low-temperature range with a very high Q<sub>10</sub>. The TRPM8 channel therefore shows a different sensitivity in several temperature ranges, which is also typical for cold-sensitive A $\delta$  fibers (Fig. 10).

The warm-sensitive TRPV3 is predominantly expressed in skin keratinocytes but also in the tongue, dorsal root ganglia, spinal cord, and brain (48, 54, 55, 148).

Figure 12 shows a Van 't Hoff plot obtained from the equilibrium constant,  $K_{\rm eq}$ , of wild-type mouse TRPV3 reconstituted into lipid nanodiscs. Above a critical temperature at  $\sim$ 36°C, the equilibrium constant increases rapidly with temperature ( $Q_{10} = 27.0 \pm 7.4$ ). The limited number of data points did not allow the T<sub>C</sub> to be determined with high accuracy. For the same reason, the existence of further critical temperatures below 36°C cannot be ruled out. Nevertheless, the assumption  $T_C \approx T_{B,mouse} \approx T_W = 36.32^{\circ} \text{C (p2}_{02}\text{-3}_{31})$  appears reasonable. This transition is accompanied by changes in gating enthalpy and entropy of  $\Delta\Delta H = 91.2 \pm 3.6 \text{ kcal mol}^{-1}$ and  $\Delta\Delta S = 287.5 \pm 11.7$  cal mol<sup>-1</sup> K<sup>-1</sup>, respectively (54). Rotational transitions,  $p2_{02}$ - $3_{31}$  (215.13 cm<sup>-1</sup>) at  $T_W = 36.32$ °C, absorb an energy of 0.62 kcal  $\text{mol}^{-1}$ . According to Eq. 1 and Eq. 2 a sum of 147 transitions of free water molecules per tetramer (~37 per monomer) would be equivalent to this enthalpy jump.

In their cryogenic electron microscopy (cryo-EM) studies of TRPV3 reconstituted in nanodiscs, Nadezhdin et al. (54) identified two distinct responses to heat depending on the type of nanodisc used, one corresponding to the canonical open state and a one in an intermediate conformational state that they interpret as sensitized (activated but still closed).

Since their heat activation protocol involves oscillation between 25°C and 42°C, crossing the major kink in temperature regimes discussed above, it is tempting to speculate that their sensitized state may share features with the high-Q<sub>10</sub> state defined by the Van 't Hoff plot. Notably, the closed-tosensitized transition involves secondary structure changes and rigid-body motions together affecting a large portion of the molecule, which seems consistent with the distributed nature of a solvent-mediated effect, whereas the actual channel opening transition was more localized. Obviously, cryo-EM would only be able to resolve temperature-dependent structural changes relaxing slowly compared to the cryocooling kinetics.

The TRPV1 channel (VR1) is sensitive to noxious heat (Fig. 13) (56, 113, 149). Rat TRPV1 channels (57) were expressed in oocytes as described by Caterina et al. (49), and singlechannel activity was measured by patch-clamping.

The authors' linear regression (149) between 40°C and 50°C (black line in Fig. 13) yielded a gating enthalpy of 150 ± 13 kcal/mol. As with the VRPM8 channels, it seems possible to identify more than one temperature regime. Accordingly, the channel activity switches between higher enthalpy (red dashed lines in Fig. 13) and lower enthalpy  $Q_{10}$  regimes (blue dashed line).

# IWQ mechanism of temperature-induced switching of TRP channel Activity.

The molecular mechanisms responsible for thermally activating TRP channels remain to be fully elucidated, but available data indicate that it involves conformational changes in different regions of the three-dimensional (3-D) structure as well as allosteric interactions (54) (Fig. 14). Thermodynamic considerations suggest that, assuming only a single openclosed transition, channel gating should be temperature dependent, favoring similar conformational changes for both heat and cold stimulation. This is due to the temperature dependence of the heat capacity change at constant pressure  $\Delta C_p$  (50) modulating  $\Delta H$  and  $\Delta S$  and hence  $K_{eq}$  of the opening transition. An increase in heat capacity upon

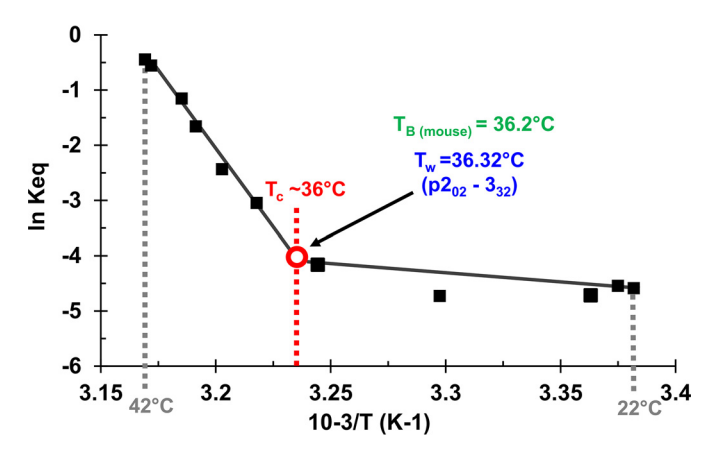
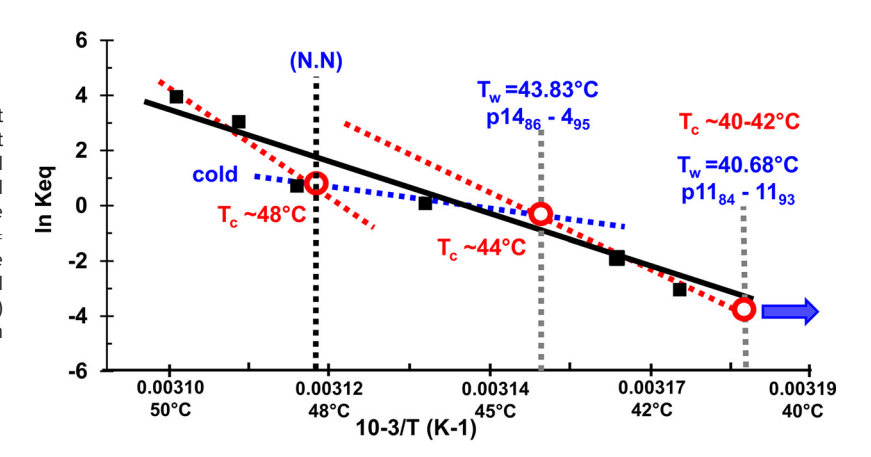


Figure 12. Warm-sensitive TRPV3: TRPV3 is thermosensitive in the range of temperatures between TRPM8 and TRPV1. The Van 't Hoff plot of the equilibrium constant ( $K_{eq}$ ) measured by patch-clamping reveals 2  $Q_{10}$ regimes separated by a kink at critical temperature T<sub>C</sub> ~36°C corresponding to mouse body temperature  $T_{B,mouse} = 36.2^{\circ}\text{C}$  and critical temperature  $T_C = 36.32^{\circ}C$  (p2<sub>02</sub>-3<sub>31</sub>) (n = 19 independent experiments). Used with permission from Ref. 54.

Figure 13. Noxious heat sensitive TRPV1: Shown is a Van 't Hoff plot generated from the equilibrium constant  $K_{eq}$  for rat TRPV1 channels expressed in oocytes (49). Single-channel inside-out patch clamp recordings were taken. Individual TRPV1 channel activity started between critical temperature  $T_C$   $\sim$ 40 and 42°C with reference temperature  $T_W$  =  $40,68^{\circ}$ C (p11<sub>84</sub>-11<sub>93</sub>). While the authors performed a simple linear regression, our detailed analysis revealed 2 additional critical temperatures,  $T_C = 44^{\circ}C$  ( $T_W = 43.83^{\circ}C$ , p14<sub>86</sub>-14<sub>96</sub>) and  $T_C=48^{\circ}C$  (T  $_W=\bar{N}.N.$  ), and 4  $Q_{10}$  regimes. Used with permission from Ref. 149 (Figure 2C).



channel opening was proposed to be caused by exposure of  $\sim$ 50 nonpolar hydrophobic side chains (10–20 per TRP protomer), representing <2% of all side chains in typical TRP channels. However, the experimental data discussed above (Fig. 11, Fig. 12, Fig. 13) indicate the presence of several states featuring individual temperature sensitivities, which correspond to slightly different closed and open structures. Within each Q<sub>10</sub> interval, the Clapham and Miller model (50) should apply in principle. However, the Van 't Hoff plot's approximate linearity and the constancy of both  $\Delta H$  and  $\Delta S$  within these intervals suggest that the influence of  $\Delta C_p$  is minimal at best. In contrast, abrupt changes in specific heat are likely associated with transitions between different Q<sub>10</sub> regimes (Fig. 13). Such an increase in  $\Delta C_p$  is consistent with our hypothesis that IWQ transitions at discrete temperatures T<sub>W</sub> can lead to protein conformational changes involving an increase in (effective) hydrophobicity. Provided that these changes are fully reversible, the switching enthalpy is released upon return to the previous temperature regime (150).

The free energies associated with conformational changes in TRP channels are typically on the order of 100 kcal/mol (143), which is equivalent to  $\sim$ 160 water molecules absorbing 0.62 kcal/mol at the rotational transition  $p2_{02}$ -3<sub>31</sub>. Even if this is only a rough estimate, two conclusions can be drawn:

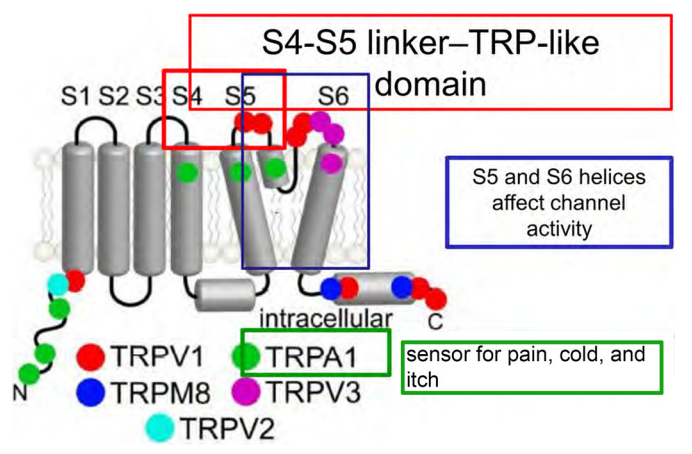


Figure 14. Regions identified as thermoactive in different TRP channels. They are mostly located in solvent-accessible portions of the protein, facing either the extracellular space or the cytosol, which is in agreement with principal interfacial water quantum-transition (IWQ) model requirements. Used with permission from Hilton et al. (58).

First, the excitation of a single free water molecule in the interface involves a nonnegligible amount of energy, even when viewed on a macromolecular scale. Second, among the thousands of water molecules comprising the first hydration layer of a large protein molecule, a small percentage undergoing quantum absorption will be sufficient to elicit a biological effect.

The water-accessible portions of TRP channels are in contact with either the extracellular medium or the cytosol (Fig. 14) (57, 58, 65).

With respect to the IWQ model, we propose that the thermally susceptible areas are located here because this is where the enthalpies required for switching can be acquired via water quantum transitions. The primary (localized) structural changes originating from energy uptake can spread as a "conformational wave" throughout the protein, similar to the closed-to-sensitized transition observed by Nadezhdin et al. (54).

Supported by allosteric coupling, these alterations will affect the entire tetrameric channel, including its transmembrane region and the gating mechanism, finally resulting in the switch between thermal regimes observed experimentally (Fig. 15).

The precise localization of the thermosensitive domains is still uncertain, and experimental studies have yielded conflicting results. Intriguingly, even a large-scale mutagenesis effort involving thousands of random exchanges in rat TRPV1 has failed to clearly map thermal susceptibility to a defined domain or region of the protein (81). The data did, however, indicate that mutations reducing hydrophobicity tended to reduce thermosensitivity but not the response to ligands. The authors interpreted their observations in terms of the heat capacity hypothesis proposed by Clapham and Miller (50). As pointed out above, this model is based on single open and closed states and, in contrast to the IWO model, cannot account for the switches between distinct temperature regimes featuring constant gating enthalpies and entropies. In fact, both the seemingly distributed nature of the effect and the dependence on apolar side chains are consistent with the postulate of the IWQ model that energy uptake at defined temperatures can be mediated by rotational activation of free water molecules. Although we expect the distribution of thermo-susceptible areas in the protein-water interface to be complex, it is certainly not random. Any given IWQ model-based rotational transition will result in a

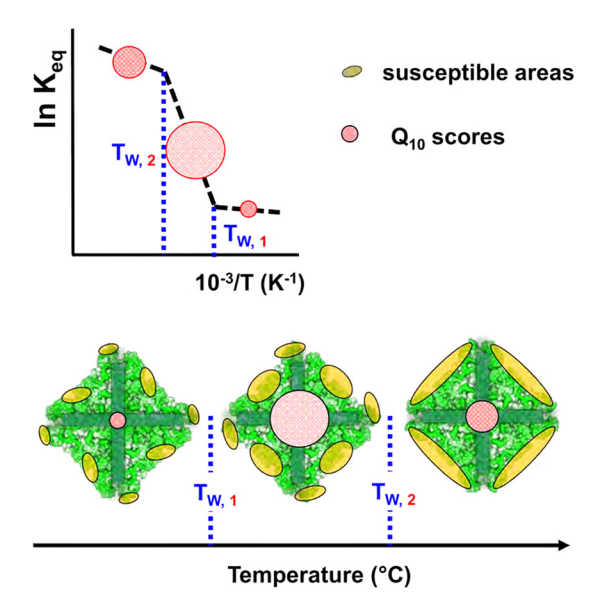


Figure 15. Bottom: the schematic representation shows a top view of a homotetrameric TRP channel (green) [compare to Hilton et al. (65)] with susceptible areas (light brown) for different  $Q_{10}$  intervals. The size and surface distribution of these areas are protein specific and change discontinuously at the interfacial water quantum-transition (IWQ) temperatures  $T_{W,1}$ and  $T_{W,2}$  (blue), concurrent with switches between  $Q_{10}$  regimes. The size of the central circle illustrates the temperature sensitivity, i.e., the  $Q_{10}$ value between the IWQ temperatures. Top: this schematic Van 't Hoff plot demonstrates typical TRP channel patch-clamp data with IWQ temperatures T<sub>W</sub> indicated. At each transition temperature, energy is absorbed locally in the susceptible areas. The allosteric interaction of these regions finally enables the switch to another  $Q_{10}$  regime.  $K_{eq}$ , equilibrium constant.

modified surface topology with an altered distribution of hot spots for generation of free water molecules, which are available for energy uptake as a different resonance temperature is reached (Fig. 15). Obviously, the information governing the thermal response of TRP channels, and hence the differences among channel types and paralogs, must ultimately be encoded in the amino acid sequence.

# **IWQ Model Implications for Thermal Homeostasis**

#### Body temperatures of homeothermic species and the IWQ temperatures.

Being homeothermic organisms, birds and mammals benefit from a strict regulation of their body temperature (T<sub>B</sub>) for constant performance and responsiveness. T<sub>B</sub> is optimized during evolution, and significant deviations from normal values can be fatal. Poikilothermic species, on the other hand, tolerate changes in their core temperatures over a wide range. The process of thermoregulation itself has been studied extensively for decades (1–3, 7, 44) and is not further considered here. Our key question is: How does a homeothermic organism "know" what the basal value of its core body temperature is, regardless of all external and internal influences (10)?

Figure 16 shows histograms of experimentally determined body temperatures for 596 mammals and 632 birds. Intriguingly, we find that both the main peaks and several secondary peaks can be assigned IWQ temperatures. In general, body temperatures are not normally distributed (Jarque–Bera test), and the frequency distribution for birds

features stronger negative skew and higher kurtosis than that of mammals. The fine structure of both distributions may be due to real variation but probably also reflects technical problems such as unequal sampling of taxa and rounding effects. Nevertheless, it is interesting to note that, despite the significant skewness, the peak value of the mammalian distribution,  $T_{B,peak,mammals} = 36.45$ °C, determined after smoothing closely matches the arithmetic mean,  $T_{B,mammals} = 36.46$ °C, both being close to the commonly-quoted standard human body temperature,  $T_{B,human} = 36.6$ °C (10).  $T_{B,peak,mammals}$  as well as  $T_{B,human}$ , in turn, correlate with the specific water rotational transition temperature  $T_W=36.32^{\circ}\text{C}$  (p2<sub>02</sub> $\rightarrow$ 3<sub>31</sub>), as postulated by the IWQ model. The maximum of the frequency distribution of birds is found at  $T_{B,peak,birds} = 42.2$ °C, and the respective IWQ temperature is  $T_W = 42.13^{\circ}C$  (p12<sub>84</sub>-12<sub>93</sub>). The Eastern bluebird (Sialia sialis) for example represents a typical avian species with a body temperature of 42.2°C.

# Hemoglobin function and body temperature: the oxygen saturation transition.

Using a variety of methods, we have demonstrated correlations between critical temperatures in the behavior of intact RBCs or Hb solutions and the body temperatures of the respective species (23). By comparing the hemoglobin sequences of these species, conserved and divergent sequence segments were identified as indicated by Zerlin and colleagues (24, 25). Hemoglobin molecular regions with higher sequence divergence tend to be closer to the surface and involve both  $\alpha$ - and  $\beta$ -subunits of the hemoglobin tetramer, including the  $\alpha$ - $\beta$  interfaces. We hypothesize that both the overall globin fold and the alpha-beta architecture of hemoglobin contain information about body temperature (70, 74, 151). Although the oxygen-binding myoglobin is a monomer, it is conceivable that it might feature a similar species-specific temperature sensitivity as observed for hemoglobin.

For homeotherm species, binding of oxygen to hemoglobin during the allosteric T-R transition (152) is a vital function. It is therefore plausible that, during the evolution of organisms, body temperatures were selected to optimally support oxygen transport by hemoglobin in the respective species. During oxygen binding, hemoglobin undergoes a reversible change in its three-dimensional structure from a tense state (T state) with lower affinity to a relaxed state (R state) featuring high affinity, due to an allosteric cooperative effect. In general, oxygen affinity of hemoglobin is well known to decrease with increasing temperature, corresponding to a shift of the oxygen binding isotherm toward higher partial pressures (153, 154).

We reasoned that the temperature-dependent transitions in structure and properties observed for hemoglobin or intact RBCs may also manifest in oxygen transport. To verify this prediction, we reassessed the temperature dependence of oxygen saturation (So<sub>2</sub>) for both mammalian (human) and avian (chicken) hemoglobin at two constant partial pressures Po<sub>2</sub>: 1) using ambient air, i.e., 150 mmHg of oxygen, and 2) 3.6% oxygen in nitrogen, corresponding to 27 mmHg of oxygen, the half-saturation pressure for human hemoglobin at human body temperature. Indeed, these recent experiments revealed sigmoidal relations. For human hemoglobin at ambient Po<sub>2</sub> this was a weak trend, with an almost linear

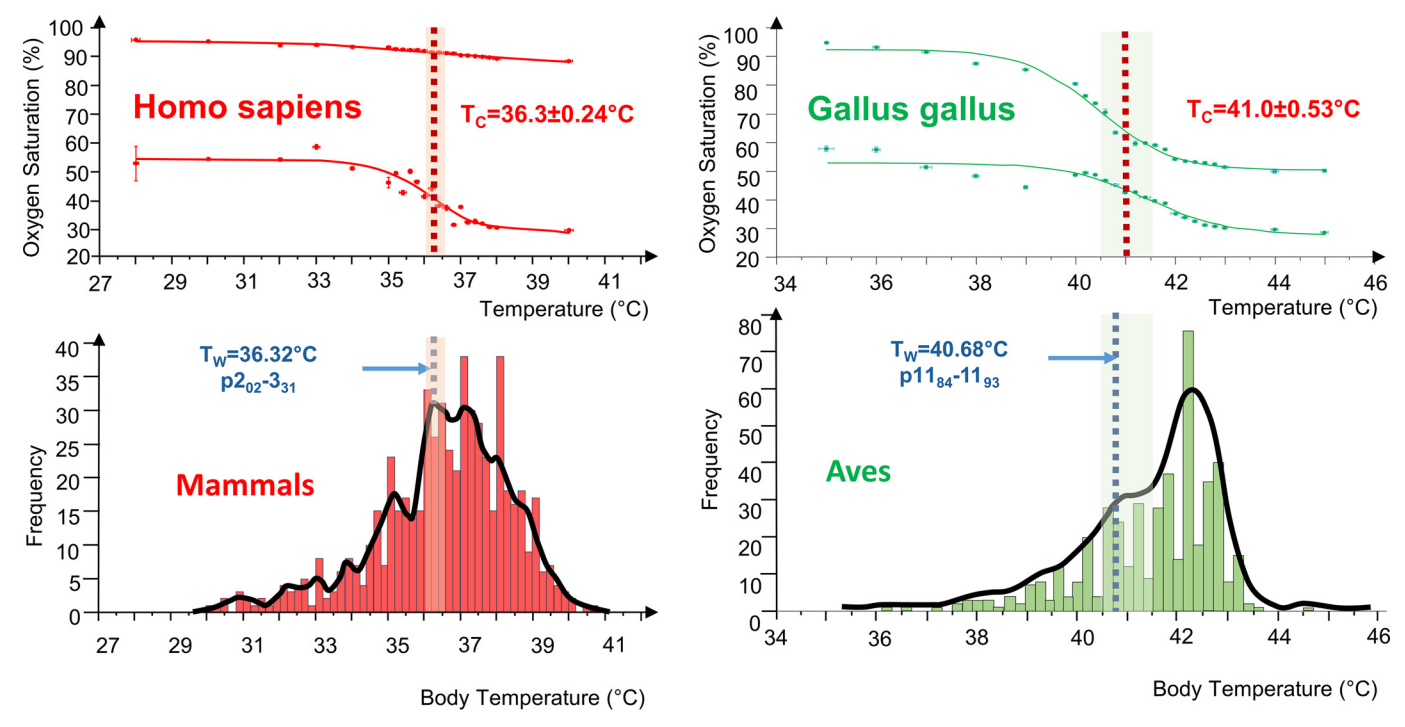


Figure 16. Oxygen saturation transition. Bottom: frequency distributions of body temperatures of mammals [N = 596, mean body temperature  $(T_{B,mean}) = 36.46 \pm 1.88^{\circ}C] \text{ and birds (N} = 464, T_{B,mean} = 41.45 \pm 1.29^{\circ}C) \text{ (mean} \pm \text{SD) (32) with the envelope curve showing the major and minor of the minor of the minor of the major and minor of the m$ maxima. Top: temperature dependence of the hemoglobin oxygen saturation (left, human; right, chicken) at atmospheric oxygen partial pressure (top curves) and 50% oxygen partial pressure (bottom curves). A sigmoidal relation was discovered in all cases. The turning points, T<sub>C</sub>, correlate remarkably well with distinct rotational transition temperatures, T<sub>W</sub>, within the limits of the measuring errors (dashed areas). The data represent mean and SD of oxygen saturation for each temperature (N = 3).

decrease in oxygen saturation of 0.67%/K (r = 0.96). Around half-saturation partial oxygen pressure, however, we observed a pronounced sigmoidal decrease (maximum slope of -8.4%/K) in human hemoglobin oxygen saturation with temperature (Fig. 16, top left). Moreover, the inflection point of this curve,  $T_C = 36.3 \pm 0.24^{\circ}$ C, was identical to the IWQ transition temperature,  $T_W = 36.32^{\circ} \text{C} \text{ (p2}_{02}\text{-}3_{31})$  and thus close to the basal value of the human body temperature,  $T_{B \text{ human}} =$ 36.6°C (10). To our surprise, we found that for chicken hemoglobin oxygen saturation exhibited a highly significant sigmoidal decrease already at ambient oxygen partial pressure, with  $T_C = 41.0 \pm 0.53$ °C and a slope at  $T_C$  of -14.3%/K, whereas at 27 mmHg of oxygen the slope at  $T_C$  (-7.7%/K) was smaller (Fig. 16, top right). Consistent with our observations with the human protein, the T<sub>C</sub> for chicken hemoglobin was, within the limits of measurement accuracy, identical to the chicken body temperature, T<sub>B,chicken</sub> (40.6–41.7°C). This value corresponds to the IWQ transition temperature  $T_W = 40.68^{\circ}C$  $(p11_{84}-11_{93}).$ 

Apparently, the oxygen binding isotherms do not just shift smoothly with temperature but display a particularly strong temperature dependence (appearing as a transition at constant partial pressure) around critical temperatures T<sub>C</sub>. To the best of our knowledge, this oxygen saturation transition has not been described before. Based on these observations, we expect similar results for other homeothermic species. If such a correlation was confirmed, this would support the generalized conjecture  $T_{C,species} = T_{B,species} = T_{W,species}$ , with T<sub>W</sub> serving as IWQ reference temperature for the respective species.

#### IWQ Model Mechanism of the Hb-Oxygen Saturation **Transition**

The process of binding oxygen in the R state is exothermic, whereas releasing oxygen in the T state is endothermic, explaining the general decrease of oxygen affinity with increasing temperature (154). If the temperature exceeds T<sub>C</sub> and the Hb oxygen saturation drops as observed, then energy must be supplied to the Hb molecule to increase the T-state probability, causing a fraction of bound oxygen to be released (Fig. 16). Considering the IWQ model, the energy required is invested to the Hb-water interface in a specific and sudden manner. The critical temperature, T<sub>C</sub>, for the oxygen saturation transition of human Hb can be assigned to the same rotational quantum transition of water ( $p2_{02}$ - $3_{31}$ , with  $T_W = 36.32$ °C) as the Hb crystal transition and the RBC passage transition discussed above. These temperature transitions of very different physical parameters exhibit similar steepness, supporting the view that they share the same cause.

In analogy to the TRP channels (Fig. 15), the IWQ energy is stored in the susceptible areas existing in R-state hemoglobin around T<sub>C</sub>. The resulting alterations in the tertiary structures of  $\alpha$ - and  $\beta$ -chains affect their elementary oxygen binding constants and/or their cooperativity, which ultimately leads to the distinct sigmoidal shape of the hemoglobin saturation curve around T<sub>C</sub>. In physiological terms, this is reminiscent of the Bohr effect (decrease of oxygen affinity upon lowering the pH) or the action of other inorganic (chloride) or organic (2,3-bisphosphoglycerate) modulators. The

difference is that rotational transitions alter the T-R equilibrium in response to a physical parameter rather than the chemical environment, and the temperature-dependent switch may or may not resemble the chemically induced ones. Regardless of structural details, the IWQ effect is likely to favor oxygen release in peripheral tissues at elevated temperatures, e.g., in skeletal muscle during exercise or under fever conditions. Whereas the temperature sensitivity of human Hb oxygen saturation is low at atmospheric Po<sub>2</sub>, or the pressure encountered in lung capillaries (100 mmHg), it increases with rising temperature to as much as 8.4%/K at  $T_C$ if Po<sub>2</sub> is close to the half-saturation level (Fig. 16). The overall result not only appears consistent with physiological demands but also is expected to usually synergize with the Bohr effect.

Another physiological effect is associated with the "work of solvation" (WoS) required during the transition from the T state to the R state (75, 84). It must be invested in the (colder) lung alveoli during Hb oxygenation to bring water molecules to the Hb surface exposed during the transition from the T state to the R state. According to Colombo et al. (75), water molecules act as allosteric effectors during Hb oxygenation (T→R transition). In the course of this conformational change, human hemoglobin requires ~60 water molecules to cover the additional surface area [420–600 Å<sup>2</sup>, roughly 4% of the solvent-accessible surface that is exposed in the relaxed state. This implies an osmotic WoS in the physiological medium of 0.2 kcal/mol. The WoS is released upon return to the T state during deoxygenation in peripheral tissues, making the process appear as a physiological heat pump. Since this process is coupled to oxygen delivery, it should share the same temperature dependence and hence be pronounced when the temperature exceeds  $T_c$ . Furthermore, part of the water absorbed during oxygen binding is released again as saturation drops at  $T \ge T_C$ .

Although monomeric myoglobin does not exhibit a T-R transition, it may still be subject to an oxygen saturation transition triggered by IWQ effects. Indeed, we were able to confirm a structural transition similar to hemoglobin via CD spectroscopy; the implications for oxygen delivery to muscle tissue are uncertain at present.

#### MATERIALS AND METHODS

For oxygen saturation measurements of hemoglobin, fresh human blood was collected via finger prick from a healthy donor into heparin-coated capillaries (BRAND, Wertheim, Germany). Brown nick chicken blood conserved in Alsever's solution was acquired from Labor Dr. Merk (Ochsenhausen, Germany). Blood samples were centrifuged with isotonic phosphate saline, and plasma was discarded. The packed red cells were hemolyzed and further diluted with 0.1 M phosphate buffer, pH 7.0 (155, 156), and centrifuged to remove the RBC membranes. The diluted hemoglobin samples were directly used for spectrophotometric analysis. The UV-VIS spectrophotometer V-550 (JASCO, Japan) was coupled with a circulation thermostat PT80 (Krüss, Hamburg, Germany), which heats both sample and reference chambers. Phosphate buffer was used as blank and reference. A 3-D printed cuvette cover that accommodates the temperature probe TDIP15 (Pyroscience, Aachen, Germany), O<sub>2</sub>

sensor OXF1100-OI (Pyroscience, Aachen, Germany), and holes for gas inlet and overpressure outlet was used. For measurements involving oxyhemoglobin, the samples were analyzed in ambient air. To create 50% oxygenated hemoglobin, the specimens were purged with a gas mixture consisting of 3.6% oxygen and 96.4% nitrogen (Linde, Pullach, Germany). The oxygen saturation was calculated by the method of Pittman and Duling (157). The oxygen saturation data were fitted to sigmoid curves to determine the inflection points with MATLAB.

#### DISCUSSION

This article presents a model for understanding discontinuities in the thermal behavior of proteins at discrete transition temperatures, with a focus on homeothermic species, in particular humans. The basic assumption is that at critical temperatures thermal energy is absorbed locally in the protein-water interface, potentially resulting in conformational changes and an associated switch in the protein's function. The surface distribution of this energy uptake is specific to the protein (and the species) as well as the transition temperature considered. As the underlying mechanism, we propose rotational quantum transitions of temporarily free water molecules in the protein-water interface (62, 64, 86, 109). This hypothesis is supported by the established rotational excitation of free water molecules in fullerene cages (93) and the experimental demonstration of such transitions in aqueous protein and DNA solutions by means of four-photon spectroscopy (90, 101, 102). Despite numerous experimental and theoretical indications in favor of the IWQ model, there remain points to be raised. A major uncertainty concerns the precise mode of rotational excitation of water molecules in the liquid state. We believe that, besides radiative energy transfer, collisional mechanisms should also be considered (61, 63, 158). The average translational kinetic energies in liquid water at thermal equilibrium should, to a good approximation, follow the equipartition theorem, yielding energy  $E = \frac{1}{3}m\overline{v^2} = \frac{1}{3}kT$  for each of the three translational degrees of freedom. Obviously, molecular translational motion in water is complicated by the presence of hydrogen-bonding networks, which may favor additional slow, collective translational modes different from those of an ideal gas; however, this will not largely affect the average energies of translation per dimension. With this premise, we can estimate the maximum energy afforded by a collision (assuming an antiparallel path) of two molecules carrying average translational energy in this particular direction as  $2 \times \frac{1}{2}kT = kT$ . On the other hand, it is worth noting that, given the broad distribution of molecular velocities predicted by Maxwell-Boltzmann statistics, the sharpness of protein thermal responses is remarkable and not completely understood. Acknowledging that keeping a protein in a higher-energy state (counteracting relaxation) will likely require a semicontinuous transfer of energy and hence a critical rate of IWQ events may offer an explanation. Resolution of this issue is awaiting future studies.

Another field to be addressed is the transfer of energy from the rotationally excited water molecules to the protein. Inverse to excitation, a rotating free water molecule may relax by radiating a far-infrared photon or by transferring energy into translational or vibrational modes, either of which can be related to heat transfer (involving neighboring solvent molecules or the protein). In structural terms, alteration of the steady-state hydrogen-bonding pattern is likely to be part of the mechanism. We assume the details to depend on the local configuration of the affected protein surface patch as well as the specific water rotational modes involved.

The IWQ model does not make any assumptions about specific structural properties of biomolecules but relies solely on the temperature dependence of the protein-water interface, including changes to the hydrogen bonding architecture and the topography of hydrophobic regions. Since the proposed mechanism represents a generic route for the water-mediated transfer of enthalpy to all kinds of cosolvents or solutes, downstream processes might be modulated in every physically possible way: in addition to favoring higher-energy states of macromolecules, as assumed in the discussion above, energy might, e.g., be utilized to overcome activation barriers, enabling transitions that are otherwise kinetically hindered though thermodynamically favorable. This model now enables us to explain the transitions observed decades ago for human RBCs as well as solutions of human hemoglobin, including the RBC passage transition, the Hb viscosity transition, and the CD secondary structure transition: in all cases the inflection point is virtually indistinguishable from the resonance temperature assigned to quantum transition  $p2_{02}$ - $3_{31}$  ( $T_W = 36.32$ °C) of *para*-water. The IWQ model implies that pronounced changes in structure and properties as a function of temperature should not be limited to soluble proteins but may analogously affect all sorts of membrane-bound proteins and ultimately any biomolecule, with potentially profound impact on all aspects of life.

As an instructive example, we reviewed available patch-clamp data on temperature-sensitive TRP channels. Unfortunately, published information on equilibrium constants in the temperature range considered here is limited. Although previous models have rationalized the general temperature dependence of gating, the remarkable switching between distinct thermal regimes at well-defined temperatures has remained enigmatic. Similar to the case of hemoglobin, the IWQ model provides a solution to the discontinuity problem by assuming that thermal energy is absorbed with particularly high efficiency at temperatures supporting rotational quantum transitions of water. This way, each type of channel can utilize its own repertoire of transition temperatures, allowing for subtype and species specificity; alterations in the amino acid sequence can widely modulate the thermal response but not the position of the candidate transition temperatures because the latter are dictated by quantum physics. Finally, based on the examples shown, we emphasize the enormous potential of patch-clamp experiments for assessing the temperature dependence of channel activity. Particular attention should be paid to the temperature accuracy directly at the cell patch.

The initial question of the paper was: Is there a physically defined reference for body temperature? We propose that it is set by the hemoglobin oxygen saturation transition. This hypothesis is supported by our recent investigation of human and chicken Hb oxygen saturation as a function of temperature. Both recordings feature a sigmoidal relation (Fig. 16, *top*), with inflection points coinciding with other hemoglobin transitions as well as with the body temperatures of the respective species. Based on these observations, temperature qualifies as another allosteric modulator causing a prominent shift in the T-R equilibrium (and hence the oxygen saturation isotherm), which is centered on basal body temperatures. The quantum transition temperature  $T_W = 36.32$ °C of the rotational transition p2<sub>02</sub>-3<sub>31</sub> therefore suggests itself as the physical reference value of human body temperature. We expect that such an assignment of body temperatures to specific rotational water transitions is also possible for other homeothermic species, but this needs to be confirmed by future investigations.

Intriguingly, our comparison across a number of mammalian and avian hemoglobins suggests that the switching temperature strongly correlates with the species' body temperature (23-25) and must hence be evolutionarily engraved into the structure of hemoglobins. If this is true, shouldn't amino acid exchanges occurring in a given species, as a result of allelic variation or spontaneous mutation, result in shifts of the reference temperature? The IWQ model clearly implies that a protein's temperatureactivity profile may be altered if an amino acid substitution affects a critical surface patch involved in energy transfer events. Axiomatically, this must apply not only to the evolution of vertebrate classes and the diversification within classes (Fig. 16) but also to intraspecies variation. It should be noted, however, that a function as fundamental as core temperature regulation is likely to be redundant, e.g., to rely on more than one sensor molecule, which should attenuate the effects of mutations in individual genes. Although we are proposing mammalian and avian body temperatures to be optimized w.r.t. oxygen transport, other proteins like TRP channels are well established to play a role in the actual temperature sensing on the organism level. Moreover, only a subset of amino acid exchanges on any protein's surface will strongly affect the response to a specific water rotational transition. As a result, the temperature response of the sensory mechanism as a whole may be quite robust toward single mutations; on the other hand, rare variations that do significantly alter the temperature response may not be recognized as such because they result in early death of the organism. To the best of our knowledge, data on genetic contributions to interindividual variation of basal body temperature in homeotherms is very limited; although indications of significant heritability do exist (159), it remains unclear whether these relate to temperature sensing or other components of thermoregulation.

Owing to the underlying physical mechanism, there is no reason to assume that IWQ transitions would not occur in the proteins of poikilothermic species. Since these have no well-defined body temperature, it is conceivable that their essential proteins are relatively stable and active over a wide range of temperatures. Nevertheless, a correlation of critical temperatures affecting certain body functions with IWQ transition temperatures can be expected. For example, the ambient temperature to which turtle eggs are exposed during hatching determines the sex of the offspring (160, 161), which means that temperature controls gene expression in these animals. Obviously, IWQ transitions might affect transcription or translation by "switching" nucleic acid-binding proteins, and previous experiments have revealed water



quantum rotation also in the presence of naked DNA (101, 162, 163). Similar considerations apply to temperaturedependent effects in other organisms, examples being microbial metabolism (164) and plant growth (165).

Regardless of the specifics of the system under study, the sharp and often unanticipated transitions in certain temperature-dependent biological processes suggest several critical requirements for future experiments: first and foremost, an accuracy of less than ±0.2°C in assessing temperature inside the sample volume studied and a sufficiently long equilibration time after technically reaching a temperature level. Furthermore, we recommend experiments with human cells and proteins or DNA at "body temperature" to be carried out in steps of  $0.2^{\circ}$ C around  $T_{\rm W} = 36.32^{\circ}$ C. Results obtained "at laboratory temperature" have their place in history and are of limited value.

In summary, we think that temperatures playing a decisive role in physiology, including the basal body temperature in homeothermic species, can be traced back to rotational quantum transitions of ortho- or para-water. The IWQ model provides a novel framework for understanding previously unexplained experimental observations. Casting the concept into a concise formula: Proteins sense and water sets critical physiological temperatures.

#### **DATA AVAILABILITY**

All data and further information are available on request from the corresponding author.

# **ACKNOWLEDGMENTS**

We express our outmost gratitude to all the scientists, colleagues, and most importantly our national and international students, who have accompanied us on this endeavor and contributed to its success.

#### GRANTS

This basic biophysical research project has been running for almost three decades, supported with the rest of the money coming from various mostly technology research proposals. The most recent funding was awarded for a collaborative project on temperature transitions in hemoglobin across different animal species, led by G.M.A. and S.D.: Competitive Research Project Gerhard M. Artmann, Samar Damiati, Department of Chemistry, University of Sharjah, Grant Number 23021440146.

#### **DISCLOSURES**

No conflicts of interest, financial or otherwise, are declared by the authors.

#### **AUTHOR CONTRIBUTIONS**

G.M.A., O.H.W., and A.T.A. conceived and designed research; G.M.A., I.S.F., and A.T.A. performed experiments; G.M.A., O.H.W., and I.S.F. analyzed data; G.M.A. and A.T.A. interpreted results of experiments; G.M.A. and S.D. prepared figures; G.M.A. and O.H.W. drafted manuscript; G.M.A., O.H.W., S.D., I.S.F., and A.T.A. edited and revised manuscript; G.M.A., O.H.W., S.D., I.S.F., and A.T.A. approved final version of manuscript.

#### REFERENCES

- Wunderlich CA. On the Temperature in Diseases: a Manual of Medical Thermometry (1st ed.). The New Sydenham Society, 1871, p. 468
- Hammel HT, Pierce JB. Regulation of Internal Body Temperature. Annu Rev Physiol 30: 641-710, 1968. doi:10.1146/annurev.ph.30. 030168.003233.
- Blatteis CM. A personal recollection: 60 years in thermoregulation. Temperature (Austin) 3: 1-7, 2016. doi:10.1080/23328940.2016.
- Wyndham CH, Atkins AR. A physiological scheme and mathematical model of temperature regulation in man. Pflugers Arch 303: 14-30, 1968, doi:10.1007/BF00586824.
- 5. Jessen C. Thermal afferents in the control of body temperature. Pharmacol Ther 28: 107-134, 1985. doi:10.1016/0163-7258(85)90085-3.
- Tan CL, Knight ZA. Regulation of body temperature by the nervous system. Neuron 98: 31-48, 2018. doi:10.1016/j.neuron.2018.02.022.
- Cabej NR. Control systems and determination of phenotypic traits in metazoans. In: Epigenetic Principles of Evolution. Elsevier, 2019.
- Moreira MO, Qu Y, Wiens JJ. Large-scale evolution of body temperatures in land vertebrates. Evol Lett 5: 484-494, 2021. doi:10.1002/ evl3.249.
- Protsiv M, Ley C, Lankester J, Hastie T, Parsonnet J. Decreasing human body temperature in the United States since the Industrial Revolution. eLife 9: e49555, 2020. doi:10.7554/eLife.49555
- Obermeyer Z, Samra JK, Mullainathan S. Individual differences in normal body temperature: longitudinal big data analysis of patient records. BMJ 359: j5468, 2017. doi:10.1136/bmj.j5468.
- McKemy DD. Temperature sensing across species. Pflugers Arch 454: 777–791, 2007. doi:10.1007/s00424-006-0199-6.
- Artmann GM, Schmid-Schoenbein H. Erythrocyte in a capillary junction (Video). 1989. https://www.youtube.com/watch?v=\_Jlu8Df-VKc.
- 13. Artmann GM, Kelemen C, Porst D, Büldt G, Chien S. Temperature transitions of protein properties in human red blood cells. Biophys J 75: 3179-3183, 1998. doi:10.1016/S0006-3495(98)77759-8.
- 14. Artmann GM. Erythrocyte aspiration into a 1.3μm pipette at 35°C (video). 1994. https://www.youtube.com/watch?v=bzYBU8oNZ-Q.
- Artmann G. Erythrocyte aspiration into a 1.3  $\mu$ m pipette at 37°C (video). 1994. https://www.youtube.com/watch?v=s3xA47T81uA. [2024 Jun 1]
- 16. Baskurt OK, Temiz A, Meiselman HJ. Effect of superoxide anions on red blood cell rheologic properties. Free Radic Biol Med 24: 102-110, 1998. doi:10.1016/S0891-5849(97)00169-X.
- 17. Weinbaum S, Li YS, Schmid-Schönbein GW. A lifetime achievement in bioengineering: Professor Shu Chien. Ann Biomed Eng 47: 2147-2150, 2019. doi:10.1007/s10439-019-02390-2.
- Fischer TM. On the energy dissipation in a tank-treading human red blood cell. Biophys J 32: 863-868, 1980. doi:10.1016/S0006-3495(80)85022-3.
- Hochmuth RM. Micropipette aspiration of living cells. J Biomech 33: 15-22, 2000. doi:10.1016/S0021-9290(99)00175-X.
- 20. Yan YB, Wang Q, He HW, Zhou HM. Protein thermal aggregation involves distinct regions: sequential events in the heat-induced unfolding and aggregation of hemoglobin. Biophys J 86: 1682-1690, 2004. doi:10.1016/S0006-3495(04)74237-X.
- 21. Artmann GM, Burns L, Canaves JM, Temiz-Artmann A, Schmid-Schönbein GW, Chien S, Maggakis-Kelemen C. Circular dichroism spectra of human hemoglobin reveal a reversible structural transition at body temperature. Eur Biophys J 33: 490-496, 2004. doi:10. 1007/s00249-004-0401-8.
- 22. Kelemen C. Analyse des phasensprungartigen Einsetzens der Passage humaner Erythrozyten durch Mikropipetten bei kritischen Temperaturen (PhD thesis). Duesseldorf: Heinrich Heine University of Duesseldorf, 1999.
- 23. Artmann GM, Digel I, Zerlin KF, Maggakis-Kelemen C, Linder P, Porst D, Kayser P, Stadler AM, Dikta G, Temiz Artmann A. Hemoglobin senses body temperature. Eur Biophys J 38: 589-600, 2009. doi:10.1007/s00249-009-0410-8.
- Digel I, Maggakis-Kelemen C, Zerlin KF, Linder P, Kasischke N, Kayser P, Porst D, Temiz Artmann A, Artmann GM. Body temperature-related structural transitions of monotremal and human hemoglobin. Biophys J 91: 3014-3021, 2006. doi:10.1529/biophysj.106. 087809.

- 25. Zerlin KF, Kasischke N, Digel I, Maggakis-Kelemen C, Temiz Artmann A, Porst D, Kayser P, Linder P, Artmann GM. Structural transition temperature of hemoglobins correlates with species' body temperature. Eur Biophys J 37: 1-10, 2007. doi:10.1007/s00249-007-0144-4
- 26. Stadler AM, Digel I, Embs JP, Unruh T, Tehei M, Zaccai G, Büldt G, Artmann GM. From powder to solution: hydration dependence of human hemoglobin dynamics correlated to body temperature. Biophys J 96: 5073-5081, 2009. doi:10.1016/j.bpj.2009.03.043.
- Stadler AM, Embs JP, Digel I, Artmann GM, Unruh T, Büldt G, Zaccai G. Cytoplasmic water and hydration layer dynamics in human red blood cells. J Am Chem Soc 130: 16852-16853, 2008. doi:10. 1021/ja807691j.
- 28. Stadler AM, van Eijck L, Demmel F, Artmann G. Macromolecular dynamics in red blood cells investigated using neutron spectroscopy. JR Soc Interface 8: 590-600, 2011. doi:10.1098/rsif.2010.0306.
- Kelemen C, Chien S, Artmann GM. Temperature transition of human hemoglobin at body temperature: effects of calcium. Biophys J 80: 2622-2630, 2001. doi:10.1016/S0006-3495(01)76232-7.
- 30. Cioni P, Strambini GB. Effect of heavy water on protein flexibility. Biophys J 82: 3246-3253, 2002. doi:10.1016/S0006-3495(02)75666-X.
- Stadler A. La Dynamique Moléculaire dans les Globules Rouges (PhD thesis). Grenoble: Université Joseph Fourier-Grenoble 1, 2009.
- Clarke A, Rothery P. Scaling of body temperature in mammals and birds. Funct Ecol 22: 58-67, 2008. doi:10.1111/j.1365-2435.2007. 01341.x.
- 33. Clarke A, Rothery P, Isaac NJ. Scaling of basal metabolic rate with body mass and temperature in mammals. J Anim Ecol 79: 610-619, 2010. doi:10.1111/j.1365-2656.2010.01672.x.
- 34. Bakker HJ. Physical chemistry: Water's response to the fear of water. Nature 491: 533-535, 2012. doi:10.1038/491533a.
- Eagle RA, Enriquez M, Grellet-Tinner G, Pérez-Huerta A, Hu D, Tütken T, Montanari S, Loyd SJ, Ramirez P, Tripati AK, Kohn MJ, Cerling TE, Chiappe LM, Eiler JM. Isotopic ordering in eggshells reflects body temperatures and suggests differing thermophysiology in two Cretaceous dinosaurs. Nat Commun 6: 8296, 2015. doi:10.1038/ncomms9296.
- 36. Stadler AM, Garvey CJ, Bocahut A, Sacquin-Mora S, Digel I, Schneider GJ, Natali F, Artmann GM, Zaccai G. Thermal fluctuations of haemoglobin from different species: adaptation to temperature via conformational dynamics. J R Soc Interface 9: 2845–2855, 2012. doi:10.1098/rsif.2012.0364.
- 37. Rego NB, Patel AJ. Understanding hydrophobic effects: insights from water density fluctuations. Annu Rev Condens Matter Phys 13: 303-327, 2022. doi:10.1146/annurev-conmatphys-040220-045516.
- 38. Makhatadze GI, Privalov PL. Heat capacity of proteins I. Partial molar heat capacity of individual amino acid residues in aqueous solution: hydration effect. J Mol Biol 213: 375-384, 1990. doi:10.1016/ S0022-2836(05)80197-4.
- 39. Privalov PL, Makhatadze Gl. Heat capacity of proteins II. Partial molar heat capacity of the unfolded polypeptide chain of proteins: protein unfolding effects. J Mol Biol 213: 385-391, 1990. doi:10.1016/ S0022-2836(05)80198-6.
- 40. Morrison SF, Nakamura K. Central mechanisms for thermoregulation. Annu Rev Physiol 81: 285-308, 2019. doi:10.1146/annurevphysiol-020518-114546.
- Zotterman Y. Special senses: thermal receptors. Annu Rev Physiol 15: 357-372, 1953. doi:10.1146/annurev.ph.15.030153.002041.
- 42. Riedel W, Siaplauras G, Simon E. Intra-abdominal thermosensitivity in the rabbit as compared with spinal thermosensitivity. Pflugers Arch 340: 59-70, 1973. doi:10.1007/BF00592197.
- Yeh FJara-Oseguera A, Aldrich RW. Implications of a temperaturedependent heat capacity for temperature-gated ion channels. Proc Natl Acad Sci USA 120: e2301528120, 2023 [Erratum in Proc Natl Acad Sci USA 121: e2401020121]. doi:10.1073/pnas.2301528120.
- 44. Tansey EA, Johnson CD, Johnson CD. Recent advances in thermoregulation. Adv Physiol Educ 39: 139–148, 2015. doi:10.1152/advan.
- 45. Lamas JA, Rueda-Ruzafa L, Herrera-Pérez S. Ion channels and thermosensitivity: TRP, TREK, or both? Int J Mol Sci 20: 2371, 2019.
- 46. Song K, Wang H, Kamm GB, Pohle J, Reis FD, Heppenstall P, Wende H, Siemens J. The TRPM2 channel is a hypothalamic heat sensor that limits fever and can drive hypothermia. Science 353: 1393-1398, 2016. doi:10.1126/science.aaf7537.

- 47. Julius D. TRP channels and pain. Annu Rev Cell Dev Biol 29: 355-384, 2013. doi:10.1146/annurev-cellbio-101011-155833.
- Clapham DE. TRP channels as cellular sensors. Nature 426: 517-524, 2003. doi:10.1038/nature02196.
- 49. Caterina MJ, Schumacher MA, Tominaga M, Rosen TA, Levine JD, Julius D. The capsaicin receptor: a heat-activated ion channel in the pain pathway. Nature 389: 816-824, 1997. doi:10.1038/39807.
- 50. Clapham DE, Miller C. A thermodynamic framework for understanding temperature sensing by transient receptor potential (TRP) channels. Proc Natl Acad Sci USA 108: 19492-19497, 2011. doi:10.1073/ pnas.1117485108.
- Bautista DM, Siemens J, Glazer JM, Tsuruda PR, Basbaum Al, Stucky CL, Jordt S-E, Julius D. The menthol receptor TRPM8 is the principal detector of environmental cold. Nature 448: 204-208, 2007. doi:10.1038/nature05910.
- 52. Rosenbaum T. TRP ion channel function in sensory transduction and cellular signaling cascades. In: TRP Ion Channel Function in Sensory Transduction and Cellular Signaling Cascades, edited by Liedtke W, Heller S. CRC Press/Taylor & Francis, 2007.
- 53. Mishra SK, Tisel SM, Orestes P, Bhangoo SK, Hoon MA. TRPV1-lineage neurons are required for thermal sensation. EMBO J 30: 582-593, 2011. doi:10.1038/emboj.2010.325.
- Nadezhdin KD, Neuberger A, Trofimov YA, Krylov NA, Sinica V, Kupko N, Vlachova V, Zakharian E, Efremov RG, Sobolevsky Al. Structural mechanism of heat-induced opening of a temperaturesensitive TRP channel. Nat Struct Mol Biol 28: 564-572, 2021. doi:10.1038/s41594-021-00615-4.
- 55. Singh AK, McGoldrick LL, Demirkhanyan L, Leslie M, Zakharian E, Sobolevsky Al. Structural basis of temperature sensation by the TRP channel TRPV3. Nat Struct Mol Biol 26: 994-998, 2019. doi:10.1038/ s41594-019-0318-7.
- 56. Luu DD, Owens AM, Mebrat MD, Van Horn WD. A molecular perspective on identifying TRPV1 thermosensitive regions and disentangling polymodal activation. Temperature (Austin) 10: 67-101, 2023. doi:10.1080/23328940.2021.1983354.
- Kim M, Sisco NJ, Hilton JK, Montano CM, Castro MA, Cherry BR, Levitus M, Van Horn WD. Evidence that the TRPV1 S1-S4 membrane domain contributes to thermosensing. Nat Commun 11: 4169, 2020. doi:10.1038/s41467-020-18026-2.
- Hilton JK, Rath P, Helsell CV, Beckstein O, Van Horn WD. Understanding thermosensitive transient receptor potential channels as versatile polymodal cellular sensors. Biochemistry 54: 2401-2413, 2015, doi:10.1021/acs.biochem.5b00071.
- 59. Schrödinger E. What Is Life? (1st ed). Cambridge University Press,
- Crovisier J, Leech K, Bockelée-Morvan D, Brooke TY, Hanner MS, Altieri B, Keller HU, Lellouch E. The spectrum of Comet Hale-Bopp (C/1995 O1) Observed with the Infrared Space Observatory at 2.9 astronomical units from the sun. Science 275: 1904-1907, 1997. doi:10.1126/science.275.5308.1904.
- Bunkin AF, Lyakhov GA, Nurmatov AA, Rezov AV. Four-photon spectroscopy of collective interactions between water molecules and electromagnetic radiation. Phys Rev B Condens Matter 52: 9360-9363, 1995. doi:10.1103/physrevb.52.9360.
- Chapovsky PL, Hermans LJ. Nuclear spin conversion in polyatomic molecules. Annu Rev Phys Chem 50: 315-345, 1999. doi:10.1146/ annurev.physchem.50.1.315.
- 63. Bunkin AF, Grachev VI, Lyakhov GA, Nurmatov AA. Four-photon polarization spectroscopy of water in a millimeter-wave radiation field. J Exp Theor Phys Lett 68: 283-286, 1998. doi:10.1134/1. 567860.
- Bunkin AF, Pershin SM. Observation of water isotopes and spin-isomers rotational transitions induced by four-wave mixing in liquid. J Raman Spectrosc 39: 726-729, 2008. doi:10.1002/jrs.1992.
- 65. Hilton JK, Kim M, Van Horn WD. Structural and evolutionary insights point to allosteric regulation of TRP ion channels. Acc Chem Res 52: 1643-1652, 2019. doi:10.1021/acs.accounts.9b00075.
- 66. Agre P. Aquaporin water channels. Biosci Rep 24: 127-163, 2004. doi:10.1007/s10540-005-2577-2.
- Meuwly M, Karplus M. The functional role of the hemoglobinwater interface (Preprint). 2110.03201, 2021. doi:10.48550/arXiv.
- 68. Pollack GH, Cameron IL, Wheatley DN. Water and the Cell. Springer, 2006.

- 69. Parsegian VA. Protein-water interactions. Int Rev Cytol 215: 1-31, 2002. doi:10.1016/s0074-7696(02)15003-0.
- Pal SK, Zewail AH. Dynamics of water in biological recognition. Chem Rev 104: 2099-2123, 2004. doi:10.1021/cr0206891.
- 71. Dill KA. Theory for the folding and stability of globular proteins. Biochemistry 24: 1501-1509, 1985. doi:10.1021/bi00327a032.
- 72. Kendrew JC, Bodo G, Dintzis HM, Parrish RG, Wyckoff H, Phillips DC. A three-dimensional model of the myoglobin molecule obtained by X-ray analysis. Nature 181: 662-666, 1958. doi:10.1038/181662a0.
- 73. Perutz MF, Rossmann MG, Cullis AF, Muirhead H, Will G, North **AC.** Structure of haemoglobin: a three-dimensional Fourier synthesis at 5.5-A. resolution, obtained by X-ray analysis. Nature 185: 416-422, 1960, doi:10.1038/185416a0,
- 74. Frauenfelder H, Hartmann H, Karplus M, Kuntz ID, Kuriyan J, Parak F, Petsko GA, Ringe D, Tilton RF, Connolly ML. Thermal expansion of a protein. Biochemistry 26: 254-261, 1987. doi:10.1021/
- 75. Colombo M, Rau D, Parsegian V. Protein solvation in allosteric regulation: a water effect on hemoglobin. Science 256: 655-659, 1992. doi:10.1126/science.1585178.
- Friesen AD, Matyushov DV. Local polarity excess at the interface of water with a nonpolar solute. Chem Phys Lett 511: 256–261, 2011. doi:10.1016/j.cplett.2011.06.031.
- 77. Davis JG, Gierszal KP, Wang P, Ben-Amotz D. Water structural transformation at molecular hydrophobic interfaces. Nature 491: 582-585, 2012. doi:10.1038/nature11570.
- 78. Pezzotti S, Sebastiani F, van Dam EP, Ramos S, Conti Nibali V, Schwaab G, Havenith M. Spectroscopic fingerprints of cavity formation and solute insertion as a measure of hydration entropic loss and enthalpic gain. Angew Chem Int Ed Engl 61: e202203893, 2022. doi:10.1002/anie.202203893.
- 79. Mallamace F, Corsaro C, Mallamace D, Vasi S, Vasi C, Baglioni P, Buldyrev SV, Chen SH, Stanley HE. Energy landscape in protein folding and unfolding. Proc Natl Acad Sci U S A 113: 3159-3163, 2016. doi:10.1073/pnas.1524864113.
- 80. Xi E, Venkateshwaran V, Li L, Rego N, Patel AJ, Garde S. Hydrophobicity of proteins and nanostructured solutes is governed by topographical and chemical context. Proc Natl Acad Sci USA 114: 13345-13350, 2017. doi:10.1073/pnas.1700092114.
- Sosa-Pagán JO, Iversen ES, Grandl J. TRPV1 temperature activation is specifically sensitive to strong decreases in amino acid hydrophobicity. Sci Rep 7: 549, 2017. doi:10.1038/s41598-017-00636-4.
- 82. Liu J, He X, Zhang JZ. Structure of liquid water-a dynamical mixture of tetrahedral and "ring-and-chain" like structures. Phys Chem Chem Phys 19: 11931–11936, 2017. doi:10.1039/c7cp00667e.
- 83. Timasheff SN. Protein hydration, thermodynamic binding, and preferential hydration. Biochemistry 41: 13473–13482, 2002. doi:10.1021/ bi020316e.
- 84. Bulone D, San Biagio PL, Palma-Vittorelli MB, Palma MU. The role of water in hemoglobin function and stability. Science 259: 1335-1336, 1993. doi:10.1126/science.8446903.
- 85. Rothman LS, Jacquemart D, Barbe A, Chris Benner D, Birk M, Brown LR. Carleer MR. Chackerian C Jr. Chance K. Coudert LH. Dana V, Devi VM, Flaud JM, Gamache RR, Goldman A, Hartmann JM, Jucks KW, Maki AG, Mandin JY, Massie ST, Orphal J, Perrin A, Rinsland CP, Smith MA, Tennyson J, Tolchenov RN, Toth RA, Vander Auwera J, Varanasi P, Wagner G. The HITRAN 2004 molecular spectroscopic database. J Quant Spectrosc Radiat Transf 96: 139-204, 2005. doi:10.1016/j.jqsrt.2004.10.008.
- 86. Rothman LS, Gordon IE, Barbe A, Benner DC, Bernath PF, Birk M, et al. The HITRAN 2008 molecular spectroscopic database. J Quant Spectrosc Radiat Transf 110: 533-572, 2009. doi:10.1016/j.jqsrt. 2009.02.013.
- 87. Tikhonov VI, Volkov AA. Separation of water into its ortho and para isomers. Science 296: 2363-2363, 2002. doi:10.1126/science.
- Farkas A. Orthohydrogen, Parahydrogen and Heavy Hydrogen. Nature 135: 601-602, 1935. doi:10.1038/135601a0.
- Kilaj A, Gao H, Rösch D, Rivero U, Küpper J, Willitsch S. Observation of different reactivities of para and ortho-water towards trapped diazenylium ions. Nat Commun 9: 2096, 2018. doi:10.1038/ s41467-018-04483-3.

- 90. Bunkin AF. Low-frequency spectroscopy of four-photon scattering in aqueous solutions of biopolymers. Biophysics 57: 709–715, 2012. doi:10.1134/S0006350912060036.
- Landau LD, Lifshitz EM. Theory of Elasticity (3rd ed.). Elsevier Ltd., 1986, vol. 7
- 92. Buntkowsky G, Limbach HH, Walaszek B, Adamczyk A, Xu Y, Breitzke H, Schweitzer A, Gutmann T, Wächtler M, Amadeu N, **Tietze D**, **Chaudret B**. Mechanisms of dipolar ortho/para-H<sub>2</sub>O conversion in ice. Z Phys Chem 222: 1049-1063, 2008. doi:10.1524/ zpch.2008.5359.
- Beduz C, Carravetta M, Chen JY, Concistre M, Denning M, Frunzi M, Horsewill AJ, Johannessen OG, Lawler R, Lei X, Levitt MH, Li Y, Mamone S, Murata Y, Nagel U, Nishida T, Ollivier J, Rols S, Rõõm T, Sarkar R, Turro NJ, Yang Y. Quantum rotation of ortho and parawater encapsulated in a fullerene cage. Proc Natl Acad Sci USA 109: 12894-12898, 2012. doi:10.1073/pnas.1210790109.
- Mamone S, Concistrè M, Carignani E, Meier B, Krachmalnicoff A, Johannessen OG, et al. Nuclear spin conversion of water inside fullerene cages detected by low-temperature nuclear magnetic resonance. J Chem Phys 140: 194306, 2014. doi:10.1063/1.4873343.
- Thiemann FL, Schran C, Rowe P, Müller EA, Michaelides A. Water flow in single-wall nanotubes: oxygen makes it slip, hydrogen makes it stick. ACS Nano 16: 10775-10782, 2022. doi:10.1021/acsnano. 2c02784.
- Frunzi M, Jockusch S, Chen JY, Krick Calderon RM, Lei X, Murata Y, Komatsu K, Guldi DM, Lawler RG, Turro NJ. A photochemical onoff switch for tuning the equilibrium mixture of H<sub>2</sub> nuclear spin isomers as a function of temperature. J Am Chem Soc 133: 14232-14235, 2011. doi:10.1021/ja206383n.
- 97. Zhukov SS, Balos V, Hoffman G, Alom S, Belyanchikov M, Nebioglu M, Roh S, Pronin A, Bacanu GR, Abramov P, Wolf M, Dressel M, Levitt MH, Whitby RJ, Gorshunov B, Sajadi M. Rotational coherence of encapsulated ortho and para water in fullerene-C60 revealed by time-domain terahertz spectroscopy. Sci Rep 10: 18329, 2020. doi:10.1038/s41598-020-74972-3.
- Limbach HH, Buntkowsky G, Matthes J, Gründemann S, Pery T, Walaszek B, Chaudret B. Novel insights into the mechanism of the ortho/para spin conversion of hydrogen pairs: implications for catalysis and interstellar water. ChemPhysChem 7: 551-554, 2006. doi:10. 1002/cphc.200500559.
- Ahlers J, Adams EM, Bader V, Pezzotti S, Winklhofer KF, Tatzelt J, Havenith M. The key role of solvent in condensation: mapping water in liquid-liquid phase-separated FUS. Biophys J 120: 1266–1275, 2021. doi:10.1016/j.bpj.2021.01.019.
- 100. Bunkin AF, Lyakhov GA, Nurmatov AA, Suyazov NV. Origin of lowfrequency spectrum structure of four-photon scattering in liquid water. Appl Phys B 66: 91-94, 1998. doi:10.1007/s003400050360.
- Bunkin AF, Nurmatov AA, Pershin SM, Khusainova RS, Potekhin SA. Four-photon microwave laser spectroscopy of aqueous solutions of biopolymers. Quantum Electron 37: 941–945, 2007. doi:10. 1070/QE2007v037n10ABEH013609.
- 102. Bunkin AF, Pershin SM, Khusainova RS, Potekhin SA. Spin isomeric selectivity of water molecules upon DNA hydration. Biophysics 54: 275-279, 2009. doi:10.1134/S0006350909030026.
- 103. Kautny P, Glöcklhofer F, Kader T, Mewes JM, Stöger B, Fröhlich J, Lumpi D, Plasser F. Charge-transfer states in triazole linked donoracceptor materials: strong effects of chemical modification and solvation. Phys Chem Chem Phys 19: 18055-18067, 2017. doi:10.1039/
- 104. Gawlik W, Kowalski J, Trager F, Vollmer M. New mechanism for the production of optical resonances with subnatural linewidths. Phys Rev Lett 48: 871-873, 1982. doi:10.1103/PhysRevLett.48.871.
- Andersen MF, Ryu C, Cladé P, Natarajan V, Vaziri A, Helmerson K, Phillips WD. Quantized rotation of atoms from photons with orbital angular momentum. Phys Rev Lett 97: 170406, 2006. doi:10.1103/ PhysRevLett.97.170406.
- 106. Maiuri M, Garavelli M, Cerullo G. Ultrafast spectroscopy: state of the art and open challenges. J Am Chem Soc 142: 3-15, 2020. doi:10.1021/jacs.9b10533.
- Fleming G. Chemical Applications of Ultrafast Spectroscopy (1st ed.). Oxford University Press, 1986.
- 108. Pershin SM, Bunkin AF, Golo VL. H<sub>2</sub>O monomers in channels of icelike water structures. J Exp Theor Phys 115: 1008–1011, 2012. doi:10. 1134/S1063776112130109

- 109. Pershin SM. Coincidence of rotational energy of H<sub>2</sub>O ortho-para molecules and translation energy near specific temperatures in water and ice. Phys Wave Phen 16: 15-25, 2008. doi:10.1007/s11975-
- 110. **Pershin SM.** Conversion of ortho-para H<sub>2</sub>O isomers in water and a jump in erythrocyte fluidity through a microcapillary at a temperature of 36.6±0.3°C. Phys Wave Phen 17: 241-250, 2009. doi:10.3103/ S1541308X09040025
- Prabhu NV, Sharp KA. Heat capacity in proteins. Annu Rev Phys Chem 56: 521-548, 2005. doi:10.1146/annurev.physchem.56. 092503.141202.
- Arcus VL, Prentice EJ, Hobbs JK, Mulholland AJ, Van der Kamp MW, Pudney CR, Parker EJ, Schipper LA. On the temperature dependence of enzyme-catalyzed rates. Biochemistry 55: 1681-1688, 2016. doi:10.1021/acs.biochem.5b01094.
- 113. Mugo A, Chou R, Chin F, Liu B, Jiang QX, Qin F. A suicidal mechanism for the exquisite temperature sensitivity of TRPV1. Proc Natl Acad Sci USA 120: e2300305120, 2023. doi:10.1073/pnas.2300305120.
- Sánchez-Moreno A, Guevara-Hernández E, Contreras-Cervera R, Rangel-Yescas G, Ladrón-de-Guevara E, Rosenbaum T, Islas LD. Irreversible temperature gating in trpv1 sheds light on channel activation. eife 7: e36372, 2018. doi:10.7554/eLife.36372.
- Perutz MF. Preparation of haemoglobin crystals. J Cryst Growth 2: 54-56, 1968. doi:10.1016/0022-0248(68)90071-7.
- Perutz MF, Muirhead H, Cox JM, Goaman LC, Mathews FS, McGandy EL, Webb LE. Three-dimensional Fourier synthesis of horse oxyhaemoglobin at 2.8 Å resolution: (I) X-ray analysis. Nature 219: 29-32, 1968. doi:10.1038/219029a0.
- Perutz MF. X-ray analysis of hemoglobin. Science 140: 863-869, 1963. doi:10.1126/science.140.3569.863.
- Artmann GM. Microscopic photometric quantification of stiffness and relaxation time of red blood cells in a flow chamber. Biorheology 32: 553-570, 1995. doi:10.1016/0006-355X(95)00032-5.
- Hochmuth RM, Buxbaum KL, Evans EA. Temperature dependence of the viscoelastic recovery of red cell membrane. Biophys J 29: 177-182, 1980. doi:10.1016/S0006-3495(80)85124-1.
- 120. **Doster W. Longeville S.** Microscopic diffusion and hydrodynamic interactions of hemoglobin in red blood cells. Biophys J 93: 1360-1368, 2007. doi:10.1529/biophysj.106.097956.
- Kim Y, Shim H, Kim K, Park HJ, Jang S, Park YK. Profiling individual human red blood cells using common-path diffraction optical tomography. Sci Rep 4: 6659, 2014. Oct 17, doi:10.1038/srep06659.
- Wang J, Bratko D, Luzar A. Probing surface tension additivity on chemically heterogeneous surfaces by a molecular approach. Proc Natl Acad Sci USA 108: 6374-6379, 2011. doi:10.1073/pnas. 1014970108.
- 123. Artmann GM. Methodische und experimentelle Beiträge zur Analyse der Ruheform, der Verformung und der Integrität humaner Erythrozyten (Thesis). Ilmenau, Germany: Technische Universität Ilmenau, 1998.
- 124. Uversky VN, Finkelstein AV. Life in phases: intra-and inter-molecular phase transitions in protein solutions. Biomolecules 9: 842, 2019. doi:10.3390/biom9120842.
- 125. Greenfield NJ. Using circular dichroism spectra to estimate protein secondary structure. Nat Protoc 1: 2876-2890, 2006. doi:10.1038/ nprot.2006.202.
- 126. Conti Nibali V, Pezzotti S, Sebastiani F, Galimberti DR, Schwaab G, Heyden M, Gaigeot M-P, Havenith M. Wrapping up hydrophobic hydration: locality matters. J Phys Chem Lett 11: 4809–4816, 2020. doi:10.1021/acs.jpclett.0c00846.
- 127. Adams EM, Pezzotti S, Ahlers J, Rüttermann M, Levin M, Goldenzweig A, Peleg Y, Fleishman SJ, Sagi I, Havenith M. Local mutations can serve as a game changer for global protein solvent interaction. JACS Au 1: 1076-1085, 2021. doi:10.1021/jacsau.1c00155.
- 128. Gevorkian SG, Allahverdyan AE, Gevorgyan DS, Hu CK. Glassy state of native collagen fibril? Europhys Lett 95: 23001, 2011. doi:10. 1209/0295-5075/95/23001.
- 129. Gevorkian SG, Allahverdyan AE, Gevorgyan DS, Hu CK. Thermalinduced force release in oxyhemoglobin. Sci Rep 5: 13064, 2015. doi:10.1038/srep13064.
- 130. Morozov V, Morozova T. Viscoelastic properties of protein crystals: triclinic crystals of hen egg white lysozyme in different conditions. Biopolymers 20: 451-467, 1981. doi:10.1002/bip.1981.360200304.

- Kapil V, Schran C, Zen A, Chen J, Pickard CJ, Michaelides A. The first-principles phase diagram of monolayer nanoconfined water. Nature 609: 512-516, 2022. doi:10.1038/s41586-022-05036-x.
- 132. Ma WJ, Hu CK. Physical mechanism for biopolymers to aggregate and maintain in non-equilibrium states. Sci Rep 7: 3105, 2017. doi:10. 1038/s41598-017-03136-7.
- 133. Pezzotti S, König B, Ramos S, Schwaab G, Havenith M. Liquid-liquid phase separation? Ask the water! J Phys Chem Lett 14: 1556-1563, 2023. doi:10.1021/acs.jpclett.2c02697.
- Bartfai T, Conti B. Fever. ScientificWorldJournal 10: 490–503, 2010. doi:10.1100/tsw.2010.50.
- 135. Blatteis CM. Endotoxic fever: new concepts of its regulation suggest new approaches to its management. Pharmacol Ther 111: 194-223, 2006. doi:10.1016/j.pharmthera.2005.10.013.
- 136. Diver MM, Lin King JV, Julius D, Cheng Y. Sensory TRP channels in three dimensions. Annu Rev Biochem 91: 629-649, 2022. doi:10. 1146/annurev-biochem-032620-105738.
- 137. Yarmolinsky DA, Peng Y, Pogorzala LA, Rutlin M, Hoon MA, Zuker **CS.** Coding and plasticity in the mammalian thermosensory system. Neuron 92: 1079-1092, 2016. doi:10.1016/j.neuron.2016.10.021.
- 138. **Schepers RJ**, **Ringkamp M.** Thermoreceptors and thermosensitive afferents. Neurosci Biobehav Rev 33: 205-212, 2009. doi:10.1016/j. neubiorev.2008.07.009.
- Tominaga M, Caterina MJ, Malmberg AB, Rosen TA, Gilbert H, Skinner K, Raumann BE, Basbaum AI, Julius D. The cloned capsaicin receptor integrates multiple pain-producing stimuli. Neuron. 21: 531-543, 1998. doi:10.1016/s0896-6273(00)80564-4.
- 140. Caterina MJ, Leffler A, Malmberg AB, Martin WJ, Trafton J, Petersen-Zeitz KR, Koltzenburg M, Basbaum Al, Julius D. Impaired nociception and pain sensation in mice lacking the capsaicin receptor. Science 288: 306-313, 2000. doi:10.1126/science.288.5464.306.
- Xu H, Ramsey IS, Kotecha SA, Moran MM, Chong JA, Lawson D, Ge P, Lilly J, Silos-Santiago I, Xie Y, DiStefano PS, Curtis R, Clapham **DE.** TRPV3 is a calcium-permeable temperature-sensitive cation channel. Nature 418: 181-186, 2002. doi:10.1038/nature00882
- McKemy DD, Neuhausser WM, Julius D. Identification of a cold receptor reveals a general role for TRP channels in thermosensation. Nature 416: 52-58, 2002. doi:10.1038/nature719.
- **Brauchi S, Orio P, Latorre R.** Clues to understanding cold sensation: thermodynamics and electrophysiological analysis of the cold receptor TRPM8. Proc Natl Acad Sci USA 101: 15494–15499, 2004. doi:10. 1073/pnas.0406773101.
- 144. Paricio-Montesinos R, Schwaller F, Udhayachandran A, Rau F, Walcher J, Evangelista R, Vriens J, Voets T, Poulet JF, Lewin GR. The sensory coding of warm perception. Neuron 106: 830-841.e3, 2020. doi:10.1016/j.neuron.2020.02.035.
- Voets T, Droogmans G, Wissenbach U, Janssens A, Flockerzi V, Nilius B. The principle of temperature-dependent gating in cold-and heat-sensitive TRP channels. Nature 430: 748-754, 2004. doi:10. 1038/nature02732
- 146. Nilius B, Voets T. Channelling cold reception. Nature 448: 147–148, 2007. doi:10.1038/448147a
- Vriens J, Nilius B, Voets T. Peripheral thermosensation in mammals. Nat Rev Neurosci 15: 573-589, 2014. doi:10.1038/nrn3784.
- Lei J, Yoshimoto RU, Matsui T, Amagai M, Kido MA, Tominaga M. Involvement of skin TRPV3 in temperature detection regulated by TMEM79 in mice. Nat Commun 14: 4104, 2023. doi:10.1038/s41467-023-39712-x.
- 149. Liu B, Hui K, Qin F. Thermodynamics of heat activation of single capsaicin ion channels VR1. Biophys J 85: 2988-3006, 2003. doi:10. 1016/S0006-3495(03)74719-5.
- Chowdhury S, Jarecki BW, Chanda B. A molecular framework for temperature-dependent gating of ion channels. Cell 158: 1148-1158, 2014. doi:10.1016/j.cell.2014.07.026.
- Perutz MF, Wilkinson AJ, Paoli M, Dodson GG. The stereochemical mechanism of the cooperative effects in hemoglobin revisited. Annu Rev Biophys Biomol Struct 27: 1-34, 1998. doi:10.1146/annurev. biophys.27.1.1.
- 152. Baldwin J, Chothia C. Haemoglobin: the structural changes related to ligand binding and its allosteric mechanism. J Mol Biol 129: 175-220, 1979. doi:10.1016/0022-2836(79)90277-8.
- 153. Willford DC, Hill EP. Modest effect of temperature on the porcine oxygen dissociation curve. Respir Physiol 64: 113–123, 1986. doi:10. 1016/0034-5687(86)90035-6.

- 154. Weber RE, Campbell KL. Temperature dependence of haemoglobin-oxygen affinity in heterothermic vertebrates: mechanisms and biological significance. Acta Physiol (Oxf) 202: 549-562, 2011. doi:10.1111/j.1748-1716.2010.02204.x.
- Yuan Y, Shen TJ, Gupta P, Ho NT, Simplaceanu V, Tam TC, Hofreiter M, Cooper A, Campbell KL, Ho C. A biochemical-biophysical study of hemoglobins from woolly mammoth, asian elephant, and humans. Biochemistry 50: 7350-7360, 2011. doi:10.1021/bi200777j.
- Bannai S, Sugita Y. Absorption spectra and reaction with haptoglobin of hemoglobin ( $\alpha$ -NO,  $\beta$ -unliganded). J Biol Chem 248: 7527– 7529, 1973. doi:10.1016/S0021-9258(19)43322-X.
- 157. Pittman RN, Duling BR. Measurement of percent oxyhemoglobin in the microvasculature. J Appl Physiol 38: 321-327, 1975. doi:10.1152/ jappl.1975.38.2.321.
- Bunkin AF, Nurmatov AA, Pershin SM, Vigasin AA. Four-photon 158. coherent spectroscopy of orientational motion of H<sub>2</sub>O molecules in liquid water. J Raman Spectrosc 36: 145-147, 2005. doi:10.1002/jrs.1291.
- Penfold RS, Zazzara MB, Österdahl MF, Welch C, Ni Lochlainn M, Freidin MB, Bowyer RC, Thompson E, Antonelli M, Tan YX, Sudre CH, Modat M, Murray B, Wolf J, Ourselin S, Veenith T, Lord JM, Steves CJ; GSTT Covid Collaborative. Individual factors including age, BMI, and heritable factors underlie temperature variation in sickness and in health: an observational, multi-cohort study.  $\it J$

- Gerontol A Biol Sci Med Sci 77: 1890-1897, 2022. doi:10.1093/ gerona/glab295.
- 160 Bowden RM, Paitz RT. Temperature fluctuations and maternal estrogens as critical factors for understanding temperature-dependent sex determination in nature. J Exp Zool A Ecol Integr Physiol 329: 177-184, 2018. doi:10.1002/jez.2183.
- Charnov EL, Bull J. When is sex environmentally determined? Nature 266: 828-830, 1977. doi:10.1038/266828a0.
- 162. Hadži S, Lah J. Origin of heat capacity increment in DNA folding: the hydration effect. Biochim Biophys Acta Gen Subj 1865: 129774, 2021. doi:10.1016/j.bbagen.2020.129774.
- 163. Xiong LL, Garrett MA, Buss MT, Kornfield JA, Shapiro MG. Tunable temperature-sensitive transcriptional activation based on lambda repressor. ACS Synth Biol 11: 2518-2522, 2022. doi:10.1021/ acssynbio.2c00093.
- 164. Boenigk J, Jost S, Stoeck T, Garstecki T. Differential thermal adaptation of clonal strains of a protist morphospecies originating from different climatic zones. Environ Microbiol 9: 593-602, 2007. doi:10. 1111/j.1462-2920.2006.01175.x.
- 165. Yan W. An equation for modelling the temperature response of plants using only the cardinal temperatures. Ann Bot 84: 607-614, 1999. doi:10.1006/anbo.1999.0955.